Simultaneous removal of fluoride and nitrate from an aqueous mixture and semiconductor wastewater by sodium chloride mediated electro-generated aluminas (EGAs): Conversion of recovered fluoride into fluorapatite using plasterboard waste

Tounsi H, T. Chaabane, K. Omine, V Sivasankar, H Sano, M. Hecini, A Darchen

Simultaneous removal of fluoride and nitrate from an aqueous mixture and semiconductor wastewater by sodium chloride mediated electro-generated aluminas (EGAs): Conversion of recovered fluoride into fluorapatite using plasterboard waste

H. Tounsi[1], T. Chaabane[2]*, K.Omine[3], V. Sivasankar[4]*,
H. Sano[5], M. Hecini[1], A. Darchen[6]

[1]Research Center in Semiconductor Technology for Energy (CRTSE), 2 Boulevard Frantz Fanon, BP 140, Alger – 7 Merveilles, 16038 Algiers, Algeria

[2]Reaction Engineering Laboratory (LGR) - Faculty of Mechanical and Process Engineering (FGMGP)/Environmental Department, University of Science and Technology Houari Boumédiène (USTHB), BP 32 El-Alia, 16111, Bab Ezzouar, Algiers, Algeria.

[3]Department of Civil Engineering, School of Engineering, Nagasaki University, 1-14 Bunkyo-machi Nagasaki 8528 521, Japan.

[4]Post Graduate and Research Department of Chemistry, Pachaiyappa's College (affiliated to University of Madras), Chennai 6000 030, Tamil Nadu, India

[5]Division of Chemistry and Materials Science, Department of Civil Engineering, Graduate School of Engineering, Nagasaki University, Nagasaki 8528 521, Japan

[6]UMR CNRS n°6226, Institut des Sciences Chimiques de Rennes, ENSCR, 11 Allée de Beaulieu, CS 50837, 35708 Rennes Cedex 7, France.

*Corresponding authors

E-mail addresses: tchaabane@usthb.dz

tfkchaabane@yahoo.fr (T. Chaabane)

sivshri.20@gmail.com (V. Sivasankar)

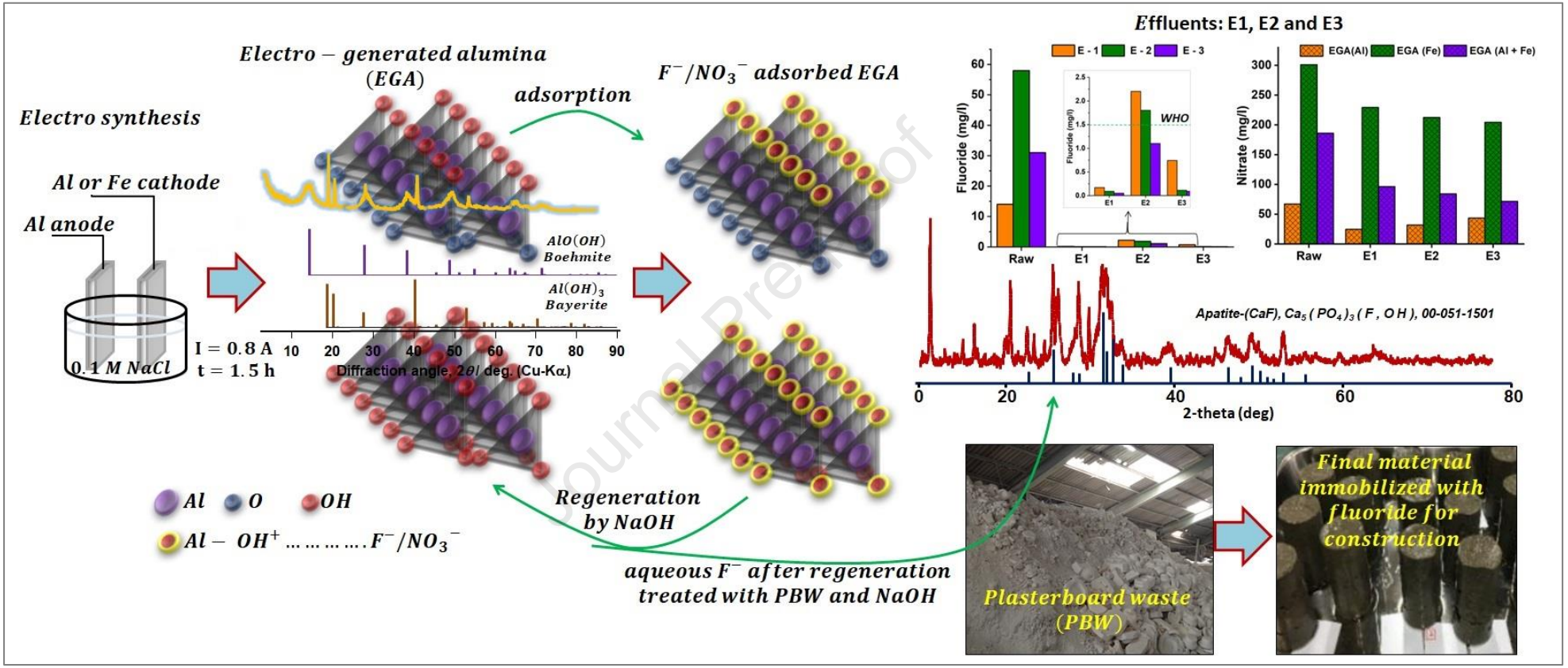
Electro synthesis
Al or Fe cathode
Al anode
0.1 M NaCl
I = 0.8 A
t = 1.5 h
Electro – generated alumina (EGA)
adsorption
F⁻/NO₃⁻ adsorbed EGA
AlO(OH) Boehmite
Al(OH)₃ Bayerite
Diffraction angle, 2θ/ deg. (Cu-Kα)
Al O OH
Al – OH⁺ ……. F⁻/NO₃⁻
Regeneration by NaOH
aqueous F⁻ after regeneration treated with PBW and NaOH
Effluents: E1, E2 and E3
E - 1 E - 2 E - 3
Fluoride (mg/l)
WHO
Raw E1 E2 E3
EGA(Al) EGA (Fe) EGA (Al + Fe)
Nitrate (mg/l)
Apatite-(CaF), Ca5 (PO4)3 (F , O H), 00-051-1501
2-theta (deg)
Plasterboard waste (PBW)
Final material immobilized with fluoride for construction

Abstract

Electro-generated aluminas (EGAs) were synthesized using sodium chloride electrolyte of 100 mM with Al/Al and Al/Fe electrodes operated at 800 mA for 1.5 h. The synthesized mesoporous EGAs, EGA (Al) and EGA (Fe) belonging to H2 type hysteresis contain the boehmite and bayerite phases as confirmed by XRD analysis and whose proportions are estimated to be 49.6±0.3% and 50.4±0.3% respectively by thermo-gravimetric study. The batch adsorption studies were conducted using the binary (F^-/NO_3^-) mixture from which the adsorption efficiency was studied as a function of time (0 – 60 min), pH (3 – 10), initial concentration of fluoride or nitrate (100, 300, 500 and 1000 mgL^{-1}) and temperature (15°C, 25°C, 35°C and 45°C) using EGA (Al) and EGA (Fe) adsorbents. The adsorptive removal of fluoride and nitrate from real effluent samples using EGAs was significant particularly in effluents E1 and E3 with residual concentrations within the safe limit of World Health Organization (WHO). Regeneration using 100 mM NaOH was quite consistent up to five consecutive cycles and the recovered fluoride was converted into fluorapatite. Taking into account the regeneration aspect, the cost analysis showed that one gram EGA (Al) and EGA (Fe) was 0.464 USD and 0.508 USD respectively. The endothermic nature of adsorption through chemical forces was confirmed by the compliance of pseudo – second – order (kinetic), Langmuir and DKR (isotherm) models ($R^2 \approx 0.99$) along with thermodynamic parameters. Characterization of EGAs using FTIR, FESEM, XRD, XPS and BET was done to understand the adsorptive behavior between EGAs and the adsorbate (F^-/NO_3^-) ions. The exhausted EGAs after fifth cycle of regeneration was mixed with ariake clay, plasterboard waste and cement in proper proportions and, made as specimens for the construction of bank bodies.

Key words: Electro-generated alumina, Fluoride and nitrate removal, Semiconductor wastewater, characterizations, Adsorption kinetics and isotherms, Fluorapatite

1. Introduction

Wastewater from a semiconductor industry is highly detrimental and a threat to water safety. The development of semiconductor industries is although significant; the treatment of generated wastewater is equally envisaged. The treatment of semiconductor wastewater becomes inevitable for the safety of mankind and the environment. The fabrication of silicon nanostructures based on stain etching by oxidants such as hydrofluoric and nitric acids in the

development of electronic and energy devices in industries (Ayat et al., 2014) discharge wastewater with high fluoride and nitrate concentrations. After the advent and growth of semiconductor industry, the global water quantity of USD 1973 million in 2017 is expected to reach USD 3258 million by 2024 (Expert_Market_Research, 2022). Sim et al., (2023) reported in view of the semiconductor wastewater treatment processes and deemed that the fluoride removal in wastewater is limited. Hence, it becomes quintessential to manage the consumption (~ 40%) of ultra-pure water for rinsing and cleaning operations during the production process (Teow et al., 2022) and the environmental risk of discharging wastewater as well. Contemporarily, the new energy technologies such as photovoltaic (PV) energy conversion systems gear up with spellbound innovations are focussed at the advent of industrial ventures during the last decade. The PV based energy is renewable and green albeit the wastewater resulting from the production process contains high fluoride and nitrate concentrations due to the application of buffered oxide etchant (BOE) using HF/HNO_3 acids. The presence of fluoride and nitrate in the wastewater from PV industries was reported to be high in the range of 500 – 2000 mg/L (Billenkamp, 2011; Drouiche et al., 2013). In Algeria, the discharge standards for wastewater with fluoride and nitrate are 15 mg/L and 50 mg/L respectively. The prolonged exposure fluoride results in teeth mottling, bones softening, tendons and ligaments ossification and, neurological damages (Aoudj et al., 2012). Nitrate is able to interfere with the ability of red blood cells to transport oxygen by causing respiratory and heart problems (Shen et al., 2018). Problems like methaemoglobinaemia, infant mortality, stomach cancer, birth defects and hypertension due to nitrate are also reported (Belkada et al., 2018). It is known to be carcinogenic on combining with amino acids as nitrosamine in digestive tract (Shick et al., 2010).

Among the above treatment technologies, adsorption is of more interest due to removal efficiency and treatment cost. Alumina based adsorbents are focussed in the adsorptive removal of various toxic pollutants including fluoride and nitrate. In particular, the modified forms of alumina in fluoride removal such as amorphous porous layered – Al_2O_3 (Yang et al., 2020), hierarchical porous – Al_2O_3 – MgO nano sheets (Yang et al., 2024), alumina modified with alum (Adu-Boahene et al., 2023), ozone activated alumina (de Paula et al., 2023), core shell boehmite (Huang et al., 2020), Mg-Al and Zn-Al layered double hydroxides (Hosni and Srasra, 2008) and highly porous activated alumina (Yu et al., 2023) are reported. On the other hand, magnetic $Al_2O_3/ZrO_2/Fe_3O_4$ nano composite (Kassahun et al., 2023) and nZVI/LDH composite (Pei et al., 2024) are applied in the removal of nitrate from water.

Furthermore, the simultaneous removal of nitrate along with chromium (Li et al., 2019), phosphate (Wu et al., 2019) and arsenic (Raj et al., 2023) was reported.

Fluoride removal from semiconductor and solar cell manufacturing industrial wastewater by electrocoagulation-adsorption (Jalil et al., 2019), electrocoagulation-flotation (Hu et al., 2005), chemical precipitation (Innocenzi et al., 2021; Diwani et al., 2022; Ho et al., 2023), coagulation – ultra filtration (Qiu et al., 2022) and, microelectronics industrial wastewater by coagulation-chemical precipitation methods (Chang and Liu, 2007), adsorption by zirconium fumarate MOF (Kumari et al., 2023) and AlOOH (Kim et al., 2023) have been reported. Jeong et al., (2013) demonstrated about 90% removal of fluoride, nitrate and phosphate in water using ZVI – packed electrolytic cell. The removal of fluoride by sorption onto calcium phosphate and the removal of nitrate by anion exchange with the interlayer sulfate of mono sulfate from the semiconductor wastewater using cement paste column was studied (Park et al., 2008). The chemical reduction of nitrate in semiconductor acidic wastewater using zero – valent iron was studied on the basis of Eley – Rideal mechanism (Yoshino and Kawase, 2013).

The removal of fluoride and nitrate of 78.4% and 81.4% respectively by adsorption using Fe (III) – doped scoria (Pirsaheb et al., 2018) was found to be less in the fluoride removal efficiency when compared to the present work using EGAs. Belkada and coworkers (2018) made investigations on the fluoride and nitrate removal using the simulated PV industry wastewater by electro-dialysis treatment and also referred the other works on fluoride and nitrate removal from wastewater of photo – voltaic industry, fertilizer industry and semiconductor industry. However, the presence of nitrate affected the removal efficiency of fluoride was reported. In another similar electro-dialysis treatment, the removal of fluoride and nitrate was pH – independent however the salinity of water decreased the fluoride removal efficiency unlike nitrate (Aliaskari and Schafer, 2021). Although the electrochemical process (Ashoori et al., 2022) was studied in the range of 44 – 61% of simultaneous removal of fluoride and nitrate, it was expensive, for which coupling of other biological methods was suggested for cost reduction.

In continuation to our previous work (Tounsi et al., 2022) on the removal of fluoride and nitrate by electrocoagulation modelled as a continuous process, the present research contributes in the simultaneous removal of fluoride and nitrate by adsorption process using electro – generated alumina (EGAs) resulting from two different cell (Al/Al and Al/Fe) systems. Apart from the twin applications of EGAs in removing fluoride and nitrate from

aqueous solution, the removal efficiency in the case of three different wastewater samples from semiconductor research laboratory, Algeria was also performed with good results. The present sorptive profile of EGAs is quite remarkable due to its reasonable cost thanks to the regeneration process unlike the other electro-dialysis, electro-chemical and electro-coagulation processes were regeneration is not feasible. The striking aspect of the present contribution is the utilization of plasterboard waste (containing fluoride) along with the recovered fluoride resulting after the EGAs regeneration process, in the conversion of benefitting fluorapatite/hydroxyapatite compounds. EGAs after prolonged regeneration cycles were treated with plasterboard and clay for making bricks suitable for building applications. The synergistic approach is intended to disseminate the scope of zero waste and environmental sustainability.

2. Materials and methods

2.1. Chemicals

All the chemicals for the preparation of EGAs and the adsorption studies were of analytical grade and purchased from Sigma-Aldrich (France). All the solutions were prepared using double distilled water. Aluminum used for electrodes was grade 1050A of the registered international designation purchased from Ridings and Dafrodis (Bouc-Bel-Air, France). The fluoride and nitrate of sodium used in adsorption experiments were purchased from Sigma-Aldrich (France).

2.2 Preparation of electro – generated alumina (EGA)

Electrolyses were carried out in a reactor of 1.5 L of capacity with magnetic stirring. Sodium chloride of 1L (100 mM) was used with electrodes (Al/Al and Al/Fe) of 11.5 cm × 4.7 cm × 0.4 cm dimensions. With the gap between electrodes of 1 cm, the electrodes were connected to a digital DC supply (2303 GPS-type) with voltage and current range of 0–32 V and 0–4 A. Prior to electrolysis, the electrodes were made ready using the procedure detailed by Zaidi et al., 2019. The electrolysis course for the preparation of EGA (Al) and EGA (Fe) was performed with a current of 800 mA for 1.5 h. At the end of the electrolyses, the electro-generated solids were collected by filtration and then rinsed three times with distilled water under agitation (to remove excess chloride) and finally dried in an oven at 105 °C for 24 h. The electro-generated adsorbents EGA (Al) and EGA (Fe) were synthesized from the electrode systems Al/Al and Al/Fe respectively. During the electrolysis,

the aliquots of samples were taken at regular intervals for the measurement of pH (780 Metrohm pH meter), turbidity (Hach 2100Q meter) and conductivity meter (Radiometer Meterlab CDM 210). The used electrodes were rinsed with distilled water and then dried at 105 °C for one hour and finally weighed. The point of zero charge pH_{zpc} for EGAs was determined by the pH drift method (Rajkumar et al., 2019).

2.3 Batch adsorption and regeneration studies

The adsorptive removal of fluoride and nitrate from the F^-/NO_3^- mixture (100 mL) for an equilibrium time of 60 min using 1g each of EGA (Al) and EGA (Fe) was set followed by the optimization of pH conditions. The effect of a constant initial concentration of fluoride or nitrate (100 mg L^{-1}) to the varied initial concentrations of fluoride or nitrate (100, 300, 500 and 1000 mg L^{-1}) at different temperatures (15°C, 25°C, 35°C and 45°C) was studied with an optimized dose (1g), contact time (60 min) and pH of EGAs. The interference of accompanying ions such as chloride, hydrogen carbonate, carbonate, sulfate and phosphate (100 mM and 1000 mM) with the adsorption efficiency of EGAs was performed. The adsorptive profile of EGAs was validated with kinetic (pseudo – first – order, pseudo – second – order and intra – particle diffusion) models, isotherm (Langmuir, Freundlich and DKR) models and adsorption thermodynamics. The practicability of EGAs to treat a real effluent sample (arose from the silicon wafer treatment with acids followed by rinsing and neutralization obtained from the Semiconductor Research Center for Energy at Algiers, Algeria) with three different concentrations of fluoride ([E1] = 14 mg L^{-1}; [E2] = 58 mgL^{-1}; [E3] = 31 mgL^{-1}) and nitrate ([E1] = 67.3 mgL^{-1}; [E2] = 301.2 mgL^{-1}; [E3] = 186.1 mgL^{-1}) was studied. The regeneration of EGA mixture for the five consecutive cycles was performed with equal concentrations of fluoride and nitrate of 50 mg L^{-1} at pH 6.25±0.05 (for the adsorption process) using 100 mM sodium hydroxide solution (for the regeneration process). The batch adsorption studies were performed by Thomas (T – 2S) thermostatic shaking bath and Hot plate stirrer (FLHS – CD; 100~1500 rpm), Front Lab, Japan. The residual fluoride (in triplicates) was measured by Thermo Scientific Orion Versa Star (Advanced Electrochemistry) meter (Channel 1, pH/ISE) using Orion fluoride ion – selective electrode (254792-001) after its calibration using TISAB – III buffer and pH buffer solutions respectively. The concentration of nitrate anions was determined by cadmium reduction method using Hanna Multiparameter Photometer (Model HI83300).

2.4 Synthesis of fluorapatite from recovered fluoride

Diammonium hydrogen phosphate (DAHP) of 50 mM was initially prepared in a solution of 100 mL containing residual fluoride (obtained after regeneration). To which, about 5 g of Plaster board waste (PBW) was added and stirred at 600 rpm and maintained in an electric furnace (Yamato Model FO300, Japan) at 303 K for 2 h. The resulting solid was washed (with distilled water), filtered and dried at 110±5°C for further characterizations.

2.5 Making specimens with exhausted EGAs

Cylindrical specimens of 100 mm height and 50 mm diameter were made using 200 kg/cm^3 of plasterboard waste (PBW), 75 kg/cm^3 of fly ash (FA), 50 kg/cm^3 of cement and 120 % Ariake clay (AC) mixed with an amount of 50 g EGA. Then the test specimens were covered with polyethylene to prevent evaporation and moisture absorption and maintained at constant temperature (25±3°C) and humidity (90±3%) in a thermo - hygrostat. These stabilized specimens were subjected for uniaxial compression tests after the curing period of 28 days.

2.6 Characterization studies

The electro-generated alumina was characterized for identifying the various vibrational modes using Fourier Transform Infrared spectroscopy with ThermoNicolet Nexus 670 NT FT – IR equipped with Attenuated Total Reflectance (ATR) spectrophotometer. The X – ray diffraction patterns and the phase identification for the EGAs were recorded using Rigaku, MiniFlex 600 Benchtop XRD (operated using 0.625 DS and 10 mm HIS with SS of 13.0 mm at 40 kV and 15 mA) and PDXL2 (Rigaku) software respectively. XPS analyses were performed using KRATOS Axis Ultra DLD (Kratos Analytical, Manchester, United Kingdom). The surface morphology of EGAs was recorded by FE – SEM (JEOL JSM – 7500FAM) and the EDS analysis was done to study the mass percentage of aluminium, oxygen and fluoride before and after the adsorption process. The physical and structural characteristics for the EGAs were determined by nitrogen adsorption/desorption at 77.5 K using Micromeritics ASAP 2020 surface area and porosity size analyzer. The thermo gravimetric (TGA) analyses were carried out using TG – EGA equipment with thermo gravimetric analyzer (TG: Shimadzu: TGA – 50H, resolution – 1 µg), non – dispersive infrared gas analysis apparatus (NDIR; Shimadzu: CGT – 7000, ranges CO: 0 – 100 ppm, CO_2 – 0 – 1000 ppm, ±2 % f.s.). The obtained data were analysed by the program created using IgorPro® and performed for the TG mass correction and synchronous processing along with fixed – quantity compensation processing of gas analysis (Sano, 2008).

3. Results and discussion

After the electrolysis process controlled at the current of 0.8 A for 1.5 h, the mass loss for the anode was 1.748 g and 1.717 g for EGA (Al) and EGA (Fe) respectively. Based on the dissolved aluminium in solution, the corresponding experimental yields of 7.6 g (Al/Al) and 3.1 g (Al/Fe) were obtained. The increase in the pH during the electrolysis process can be demonstrated due to the substitution of chloride ion by ejecting the hydroxide ion (Tchomgui-Kamga et al., 2013) into solution (Eq. 1 and 2). However, the pH increase for EGA (Fe) was less than that of EGA (Al) in pertinent to that of controlled substitution and lessened ejection of chloride and hydroxyl groups respectively.

$$AlO(OH) + Cl^- \rightarrow AlO(Cl) + OH^- \quad \text{..... (1)}$$

$$Al(OH)_3 + Cl^- \rightarrow Al(OH)_2Cl + OH^- \quad \text{..... (2)}$$

Similarly, the increase in conductivity attributes the greater mobility due to the ejection of hydroxide ions than that of chloride ions. The linear increase in turbidity indicates the formation of homogenous particles of EGA during the electrolysis process (Fig. S1).

3.1 Equilibrium time of adsorption

The adsorption of fluoride and nitrate from the F^-/NO_3^- mixture as a function of contact time is shown in Fig. 1 (A and B). It is apparent that both the fluoride and nitrate adsorption becomes significant with the adsorption rates for fluoride (EGA (Al) – 1.84 mg min^{-1}; EGA (Fe) – 1.86 mg min^{-1}) and nitrate (EGA (Al) – 11.1 mg min^{-1}; EGA (Fe) – 10 mg min^{-1}) during the first five minutes. Subsequently, the rates drop down to 0.003 – 0.004 mg min^{-1} (fluoride) and 0.21 – 0.43 mg min^{-1} (nitrate) till the equilibrium was established at the end of 60 minutes. The rapid adsorption phase took place with the escalation of active surface protonated sites of EGAs in the first five minutes and then becomes almost linear (Chu et al., 2022) afterwards due to depletion of active sites by attaining the equilibrium after 60 minutes.

3.2 Effect of pH on the adsorption of F^- and NO_3^- from the F^-/NO_3^- mixture

Firstly, pH of the solution plays a significant role in the adsorption of soluble ions onto the adsorbent mainly by interfacial interaction (Karimi and Rahbar-Kelishami, 2022). From the F^-/NO_3^- mixture, the adsorption of fluoride and nitrate increased between pH 6.02±0.03 and pH 7.03±0.04 and decreased thereafter. The highest fluoride and nitrate removals were recorded as 99.50±0.04 % and 83±1 % respectively on using EGA (Al) and EGA (Fe)

adsorbents as shown in Fig. 1 (A and B). The difference in the efficiencies of fluoride removal for the two adsorbents looks insignificant (0.04 – 0.5 mg g^{-1}) albeit the difference in the nitrate removal seems appreciable (7.3 – 11 mg g^{-1}). The pH_{zpc} of EGA (Al) and EGA (Fe) was determined with 7.6 and 8.3 respectively. In respect of the pH less than pH_{zpc}, the electrostatic force of attraction becomes dominant (Eq. (3) – (6)) and operative between the protonated O – H bound to Al – O groups and the $F^-/NO_3{}^-$ ions present in the mixture (You et al., 2019). It is significant to corroborate that the surface concentration of $F^-/NO_3{}^-$ was greater than the bulk concentration at $pH < pH_{zpc}$ but lower at $pH > pH_{zpc}$ (Lin et al., 2020). However, either the increase in the competition between the fluoride/nitrate and the hydroxyl ions or the repulsion of fluoride/nitrate by the negatively charged EGAs surface leads to the diminution of removal efficiency at pH particularly greater than the pH_{zpc}. Guan et al., 2022 studied that the adsorption ability of alumina decreases as a consequence of surface hydroxylation based on density functional theory. Conspicuously, the nitrate removal efficiency being higher for EGA (Fe) than EGA (Al) may be pertinent to higher pH_{zpc} value leading to the availability of positive charges at pH values greater than 7. In support of this observation, Fritche (1993) reported that the presence of OH^-ions, the caustic agent becomes responsible for the removal of $NO_3{}^-$ ions through ion – exchange mechanism. The present observation is in agreement with the study report by Khatamian et al., 2024.

$$AlO(OH) + H^+ \rightarrow AlO(OH_2{}^+) \quad \text{..... (3)}$$

$$AlO(OH_2{}^+) + F^- \rightarrow AlO(OH_2{}^+ \ldots\ldots\ldots\ldots\ldots F^-) \quad \text{..... (4)}$$

$$AlO(OH_2{}^+) + NO_3{}^- \rightarrow AlO(OH_2{}^+ \ldots\ldots\ldots\ldots\ldots NO_3{}^-) \quad \text{..... (5)}$$

$$AlO(OH) + NO_3{}^- \rightarrow AlO(OH) \ldots\ldots\ldots\ldots NO_3{}^- \quad \text{..... (6)}$$

3.3 Effect of initial concentrations on the adsorption of F^- and $NO_3{}^-$ from the $F^-/NO_3{}^-$ mixture

At constant initial concentration of nitrate or fluoride (100 mg L^{-1}), the effect of initial fluoride (or nitrate) concentration of 100, 300, 500 and 1000 mg L^{-1} on the adsorptive removal of fluoride at 15°C, 25°C, 35°C and 45°C was studied (Fig. S2 (A and B). On increasing the concentration of F^- *and* $NO_3{}^-$ to 1, 3, 5 and 10 times (by keeping the other at a constant concentration of 100 mgL^{-1}), the amount of adsorbed F^- or $NO_3{}^-$was increased. At the same time, the adsorption of $F^-$and $NO_3{}^-$ from the mixture was found to increase with

the increase in temperature for the four different F^-: $NO_3{}^-$ratios (1:1, 1:3, 1:5; 1:10). The adsorption quantity of fluoride by EGA (Al) and EGA (Fe) was higher than that of nitrate due to the influence of temperature and initial concentrations. Wu et al (2019) reported that the co – sorption of nitrate and phosphate develops a mutual inhibition resulting in the lessened removal efficiency of the ions. In the present study, the adsorption of fluoride onto EGA (Al) and EGA (Fe) was in the range of 2.2 – 3.1 times and 2.1 to 2.7 times greater than that of nitrate respectively. The competency for adsorption onto the surface of active sites of EGAs may be associated with the ionic radii of the competing ions especially the lesser ionic radius of fluoride (0.136 nm) dominated over that of nitrate (0.177 nm). In accordance with the present findings, the adsorption of fluoride dominated over nitrate onto mixed hydrous bismuth oxide (Ranjan and Singh, 2020). Furthermore, it was demonstrated that the competing tendency between F^- and $NO_3{}^-$ anions was less due to their monovalent nature with weaker electrostatic interaction and low affinity for adsorption sites (Gao et al., 2022) unlike the multivalent anions with greater affinity and high competing tendency (Gogoi et al., 2019). The impact of temperature on the adsorption of fluoride at varied concentrations was almost similar for EGA (Al) and EGA (Fe) whereas the adsorption of nitrate at different concentrations was little higher for EGA (Al) (1.6 – 1.9 times) than that of EGA (Fe) (1.4 – 1.63 times).

3.4 Effect of co - ions on the adsorption of $F^-$and $NO_3{}^-$from aqueous solutions

Apart from the mutual interference (between the fluoride and nitrate ions), the interference of other anions such as chloride, hydrogen carbonate, carbonate, sulfate and phosphate on the removal efficiency of fluoride and nitrate was studied (Fig. 2). The increase in the concentration of interfering ions by 10 times (100 mM to 1000 M) affected the removal rate of fluoride and nitrate for EGAs. The relative concentration of the coexisting ion and its affinity for the adsorbent are intrinsically related to the ionic radius and the charge. These factors significantly decide the competing ability of co-ions (Tao et al., 2020). The interference of sulphate against the removal of nitrate was higher up to 84% than that of fluoride of 46%. Sulphate tends to form the outer sphere complex *via* electrostatic attraction while competing for the active site on EGAs (Tor et al., 2006). The interference of phosphate on the removal of fluoride and nitrate seems almost closer between the two EGAs. The hindrance caused by phosphate ion was due to the formation of inner sphere complexation with Al of EGAs (Zheng et al., 2012). The competency of hydrogen carbonate against fluoride and nitrate on the surface of EGA (Al) was little higher (7 – 8%) than that of EGA

(Fe) with 2 – 5%. Nevertheless, the inhibition (~11%) caused by 100 mM of hydrogen carbonate solution to the adsorption of nitrate was higher than that of fluoride. The inhibition is pertinent to the fact that HCO_3^- ion is known to form inner – sphere monodentate complexes with the surface functional groups of aluminium hydroxides (John et al., 2018; Turki et al., 2023). On the other hand, the inhibition due to carbonate was higher (7 – 12%) against fluoride than that of nitrate for EGA (Fe). The presence of carbonate undergoes hydrolysis, thereby increasing the pH of the solution which hinders the sorption (Huang et al., 2020; Tie et al., 2022). The competency between chloride against fluoride and nitrate was insignificant during adsorption onto EGAs. The order of inhibition by the interfering ions during the sorption onto EGAs is as follows.

$$SO_4^{2-} > HCO_3^- > PO_4^{3-} > CO_3^{2-} > Cl^- \ (for\ nitrate\ sorption)$$

$$HCO_3^- > PO_4^{3-} > CO_3^{2-} > SO_4^{2-} > Cl^- \ (for\ fluoride\ sorption)$$

3.5 Adsorption modelling

3.5.1 Kinetic models

The various kinetic models as expressed in Eq. (7) – (9) are given below and the kinetic plots are shown in Fig. S3. In these equations, Q_t and Q_e are amounts adsorbed at a particular time (t) and equilibrium as well. The pseudo – first – order (Lagergren, 1898), pseudo – second – order (Ho and McCay, 1918) and intra – particle diffusion (Weber and Morris, 1963) rate constants are denoted as k_1 (min^{-1}), k_2 ($g\ mg^{-1}min^{-1}$) and k_d ($g\ mg^{-0.5}\ min^{-0.5}$) respectively. The term 'C' in Eq. (1) is the constant relating the extent of boundary layer effect.

Firstly, pseudo – first – order model validates a system of adsorption which occurs with diffusion through the interface. In the present sorption system, the pseudo – first – order rate constant (k_1) for the fluoride sorption onto EGA (Al) was two times higher than that of EGA (Fe) and, 1.86 times greater for the nitrate sorption onto EGA (Al). Based on the pseudo – first – order model, the adsorption capacity of EGAs (Al and Fe) was higher than three times for fluoride (4.459 mg g^{-1} and 4.180 mg g^{-1}) than that of nitrate (1.315 mg g^{-1} and 1.355 mg g^{-1}) from the fluoride/nitrate mixture.

$$\ln(Q_e - Q_t) = lnQ_e - k_1(t) \quad \text{..... (7)}$$

$$t/Q_t = 1/k_2Q_e^{\,2} + \frac{1}{Q_e}(t) \quad \text{..... (8)}$$

$$Q_t = k_d t^{0.5} + C \quad \text{..... (9)}$$

Secondly, pseudo – second – order model is based on the rate – limiting step being assumed to be chemisorption (Ho, 2006). Based on this model, the pseudo – second order rate constant (k_2) for fluoride sorption differs by 0.012 g mg^{-1} min^{-1} between EGA (Al) and EGA (Fe) whereas for nitrate sorption it was about 2.5 times greater for EGA (Al) than that of EGA (Fe). The highly validated pseudo – second – order model represented the adsorption capacities for fluoride with 9.862 mg g^{-1} and 9.970 mg g^{-1} for EGA (Al) and EGA (Fe) respectively. Similarly, the nitrate adsorption capacities with 68.027 mg g^{-1} and 75.758 mg g^{-1} were recorded. The initial sorption rate (h) for fluoride was observed in the close range of 33.6±1.1 mg g^{-1} min^{-1} for EGA (Al) and EGA (Fe) respectively. However, in the case of nitrate, 'h' was doubled (46.27 mg g^{-1} min^{-1}) for EGA (Al) than that of EGA (Fe). The regression coefficient values (0.999 – 1.000) were excellent in support of the pseudo – second – order model unlike the first – order model (0.864 – 0.945). The validation of the pseudo – second – order model further confirms the sorption of fluoride and nitrate through chemical forces as a result of the exchange of electrons between EGAs and fluoride/nitrate ions (Bhatnagar et al., 2010; Oulebsir et al., 2020).

The intra – particle uptake of fluoride and nitrate from the binary mixture and the corresponding pore diffusivity, especially of mesoporous and microporous nature (Allen et al., 1989), based on Weber and Morris model is investigated. The intra – particle diffusion rate constant for fluoride sorption was 1.6 times higher for EGA (Al) than that of EGA (Fe) however, the reverse was true for the nitrate sorption by two times (Table 1). Accordingly, the higher boundary layer thickness (He et al., 2020; Mahinroosta et al., 2021) during the sorption of nitrate than fluoride for the two EGAs was observed. The resistance to external mass transfer of nitrate was higher than that of fluoride may be attributed to the ionic radius of nitrate (1.79 Å) greater than that of fluoride (1.33 Å). In the present dual sorption system, the plots did not pass through the origin ($C_1 \neq 0$) and confirms that the initial film diffusion and then the intra – particle diffusion process take part in the rate determining step. The depiction of linear plots attributed the difference in the rates of mass transformation of fluoride and nitrate between the initial and final adsorption stages for the two EGAs (Mall et al., 2006). The above observations are further corroborated by the regression values (0.906 – 0.970).

3.5.2 Adsorption isotherms

The compliance of isotherm models *viz*., Langmuir (Langmuir, 1918), Freundlich (Freundlich, 1906) and DKR (Dubinin, 1960) (Fig. S4) with the sorption of fluoride and nitrate from the binary mixture is discussed as follows.

$$\frac{C_e}{Q_e} = \frac{1}{bQ^o} + \frac{C_e}{Q^o} \quad \text{..... (10)}$$

$$lnQ_e = lnK_F + \frac{1}{n} lnC_e \quad \text{..... (11)}$$

$$lnQ_e = lnQ_m - \kappa\varepsilon^2 \quad \text{..... (11a)}$$

$$\varepsilon = RTln\left(1 + \frac{1}{C_e}\right); R = 8.314\, Jmol^{-1}K^{-1}, T - Temperature \quad \text{..... (11b)}$$

$$E = \frac{1}{(2K)^{0.5}} \quad \text{..... (11c)}$$

where Q^o (mg g^{-1}) is the maximum adsorption capacity and b (Lmg^{-1}) is the Langmuir isotherm constant relating the affinity of binding sites and the energy of adsorption. On the basis of Langmuir model (Eq. 10), each adsorption site has equal energy due to homogeneous surface resulting in the monolayer sorption of fluoride and/or nitrate ions (Oulebsir et al., 2020). The plot of C_e/Q_e versus C_e gives the (Q^o) and b from the slope and the intercept respectively. The fluoride and nitrate sorption capacities (Q^o) of EGA (Fe) were greater than that of EGA (Al). The endothermic nature of sorption onto EGAs becomes evident from the sorption capacities which are proportional to the temperature. The dimensionless constant which expresses the feasibility of the Langmuir isotherm is R_L which is equal to $[\frac{1}{1+bC_0}]$. This parameter (R_L) was observed between 0 and 1 and confirms the favourable sorption of fluoride and nitrate from the binary mixture. Based on the Langmuir constant between 15°C and 45°C, the R_L values tend to decrease from the range 0.740±0.017 to 0.223±0.015 (for nitrate) and 0.642±0.116 to 0.152±0.052 (for fluoride) for the C_0 values 100 mg L^{-1} and 1000 mg L^{-1} respectively. Upon increasing the initial concentration of fluoride and nitrate the decrease in the dimensionless constant corroborated the approach of sorption from favourable to irreversible nature. Accordingly, the present observation was witnessed from the studies in which the adsorption rate constant was decreased and slows down at a higher fluoride concentration (Maity et al., 2018; Su et al., 2020). The regression coefficients corroborated the compliance of the Langmuir model in conformity with the dominant monolayer sorption of fluoride (R^2 = 0.985±0.015) and nitrate ions (R^2 = 0.965±0.025) on the surface of EGAs (Oulebsir et al., 2020; Kassahun et al., 2023).

Freundlich model (Eq. 11) provides an indirect evidence for the site (or surface) heterogeneity and the preference of binding sites in the order of decreasing energy. K_F (mg g^{-1}) and n are Freundlich constants. The surface heterogeneity (1/n) during nitrate sorption (0.51±0.04; 0.52±0.02) was higher by 0.2 folds than that of fluoride sorption (0.62±0.04; 0.60±0.03) for the two EGAs. The values for surface heterogeneity (1/n) less than 1, infers that the sorption of fluoride and nitrate is favourable onto EGAs. The fluoride adsorption capacity (K_F) increased on increasing the temperature from 15°C to 45°C for EGA (Al) and EGA (Fe) materials unlike the sorption capacity of nitrate. However, the compliance of Freundlich model seems to be less consistent than the Langmuir model based on the regression coefficient values (Table 2 and 3).

In the Dubinin – Kaganer – Radushkevich (DKR) equation (Eq. 11a – 11c), the terms Q_m, ε, κ and E are monolayer adsorption capacity (mg g^{-1}), Polanyi potential, and constant related to adsorption energy (mol^2/kJ^2) respectively. The mean free energy, E (kJ mol^{-1}) as shown in Eq. 1c is the energy which transfers 1 mole of adsorbate from infinity in solution to the surface of the adsorbent. On increasing the temperature, the monolayer adsorption capacity of fluoride increases by 36±1% for EGA (Al and Fe) along with the free energy (40.82 – 79.05 kJ mol^{-1}) of EGA (Al) greater (1.9 – 3.3 folds) than that of EGA (Fe). On the other hand, the DKR adsorption capacity during nitrate sorption increased by 74% and 58% for EGA (Al) and EGA (Fe) respectively with the increase in temperature (Table 2). However, the free energy in the case of nitrate sorption between EGA (Al) and EGA (Fe) remains closer to each other. The values of free energy greater than 16 $kJmol^{-1}$ indicated the involvement of strong chemical forces during the sorption of fluoride and nitrate ions. Similar observation was reported by Yang et al., (2024) in pertinent to chemisorption with free energy of 12. 91 kJ mol^{-1}. This model fits moderately well with the regression coefficient values after Langmuir and Freundlich isotherms.

3.6 Adsorption thermodynamics

The equations for the thermodynamic parameters associating the adsorption process are given from Eq. (12a) to Eq. (12d). The plots of lnk_d versus 1/T are shown in Fig. 3 (A & B).

$$\Delta G^0 = RTlnk_d \quad \text{……. (12a)}$$

$$\Delta G^o = \Delta H^o - T\Delta S^o \quad \text{……. (12b)}$$

$$lnk_d = \frac{\Delta S^o}{R} - \frac{\Delta H^o}{RT} \quad \text{..... (12c)}$$

$$k_d = \frac{Q_e}{C_e} \quad \text{..... (12d)}$$

$$lnk_d = \ln A_0 - (E_a/RT) \quad \text{..... (12e)}$$

The positive values of ΔH^0 during the adsorption of fluoride and nitrate indicated the endothermic nature of adsorption process with values of EGA (Fe) greater than that of EGA (Al). The enthalpy change greater than 25 $kJmol^{-1}$ during the sorption of fluoride and nitrate ions involve the governance of chemical forces as referred by Gopal and Ilango, 2007. This fact on the absolute dominance of chemical forces during sorption (Gai et al., 2021) is further supported by the values of activation energy (E_a) of 17.4 – 20.1 $kJmol^{-1}$ for EGAs as shown in Eq. (12e). In addition, the positive values of ΔH^0 was also corroborated by the fact that the energy required for the desolvation process overwhelms the exothermicity of fluoride or nitrate sorption on the surface of EGAs (He et al., 2019). Similarly, the increase in ΔS^0 values demonstrated the increase in randomness at the interface between the solid and the mixture. The increase in entropy change may be associated with the displacement of water molecules by fluoride/nitrate ions. The displacement leads to gain more translational entropy leading to the prevalence of increased randomness in the system on increasing the temperature from 288 K to 318 K (Oulebsir et al., 2020). The negative ΔG^0 values tend to become more negative on increasing the temperature and confirm the spontaneity of the adsorption of fluoride and nitrate onto the EGA (Al and Fe) materials as shown in Table – 4.

3.7 Fluoride and nitrate removal in raw effluent samples

The abatement of fluoride and nitrate ions from the real wastewater was achievable within the safe limits of 1.5 mgL^{-1} and 50 mgL^{-1} respectively using EGAs as shown in Fig. 4 (A and B). The residual fluoride in the effluents E1 and E3 were well below the permissible limit of WHO. On the other hand, the reduction of nitrate was in the range 35.4 – 63.6% (23.8 – 42.8 mgg^{-1}), 48.2 – 61.5% (89.7 – 114.5 mgg^{-1}) and 23.9 – 32.2% (71.9 – 96.9 mgg^{-1}) for the initial concentrations 67.3 mgL^{-1}, 186.1 mgL^{-1} and 301.2 mgL^{-1} respectively. The residual nitrate only in E1 was within the safe limit as prescribed by WHO. The EGA mixture was found with higher removal efficiency of fluoride and nitrate than the individual EGAs. The improved removal may be attributed to the perturbation of textural properties of EGA (Al) and EGA (Fe) in tandem. In support of the EGA mixture (combined adsorbent), Arcibar –

Orozco et al., (2018) reported the synergistic effect of zeolite and chitosan in the removal of fluoride from aqueous solution. Katheresan et al., (2018) suggested the prospects of wastewater treatment due to the combination of adsorbents. Furthermore, the application of secondary aluminium ash in removing fluoride (98.9%) from industrial wastewater was reported (Li et al., 2022). The residual levels of all other ions present in the effluent after the adsorption treatment were well within the safe limit of WHO as shown in Table – 5. The leaching of Al from EGA mixture was observed at the below detectable level in the treated semiconductor wastewater and for Fe, the leaching was estimated with the maximum value of 0.005 mgL^{-1}. The pH of the raw wastewater effluent between 6.2 and 7.7 could be attributed to the undissolved nature of EGAs during the treatment process where the pH also changes to the close range between 5.6 and 6.6.

3.8 Regeneration of EGAs

Regeneration of exhausted EGAs was performed to emphasize the continued usage of the adsorbent. The mixture of EGAs in the ratio of 1:1 containing EGA (Al) and EGA (Fe) was used during the adsorptive removal and the regeneration processes. The initial concentration of fluoride and nitrate in the solution mixture was equal with 50 mg/l each. The fluoride and nitrate removal efficiencies decreased in the range of 99 – 80% and 71 – 55% respectively at the end of fifth cycle (Fig. 4C). It is apparent that the diminution rates of fluoride (3.3% per cycle) and nitrate (3.8% per cycle) removals seem to be closer albeit the percentage removal for fluoride was quite higher than nitrate at every regeneration cycle. The resulting solution with fluoride and nitrate was utilized for the synthesis of fluorapatite which paves the way for other applications subject to conditions based on its purity.

3.9 Synthesis of fluorapatite from recovered fluoride treated with plasterboard waste

The residual fluoride in solution after regeneration was converted into fluorapatite on treatment with plaster board waste. In this way, the fluoride was recovered and converted into another compound to disclose a way for new applications. The XRD pattern (Fig. 5A) for the obtained fluorapatite is with the space group, 176:P63/m for the formula $(CaF)Ca_5(PO_4)_3F$ and the lattice parameters, a = 9.464 Å, b = 9.464 Å and c = 6.911 Å. The obtained apatite exhibited the vibrational stretching bands at 1030 and 1090 cm^{-1} (υ_3) for ${PO_4}^{3-}$ and, hydroxyl stretching around 3570 cm^{-1}. The symmetric and asymmetric stretching vibrations for ${SO_4}^{2-}$ respectively appeared at 1010±10 cm^{-1} and 1110±10 cm^{-1} along with a bending

mode for OH^- group at 1620 cm^{-1} (Fig. 5B). The shift of υ_{OH} (~3500 cm^{-1}) to lower wavenumbers by 1 to 10 cm^{-1} was stemmed out due to the hydrogen bonding between OH^- and F^-. The vibrational modes for Raman spectra of PBW were located at 1006 cm^{-1}, 485 cm^{-1}, 1182 cm^{-1} and 669 cm^{-1} for the symmetric stretching (ν_1), symmetric bending (ν_2), asymmetric stretching (ν_3) and asymmetric bending (ν_4) respectively (Sivasankar et al., 2023). The above assignments are well in agreement with the findings of Schmid et al. (2020). On treatment of recovered fluoride with PBW and DAHP, the vibrational mode at about 964±2 cm^{-1} is associated to the totally symmetric (ν_1) A_1 stretching of 'free' tetrahedral PO_4^{3-} ion. This characteristic band for hydroxyapatite was observed to be highly intense (Fig. 5D). A low intense band at 320 cm^{-1} attributed the highly stable and covalent type Ca – F bond on apatites. The SEM morphology displayed a plate like fluorapatite grains with the Ca/P ratio of 1.62 with the presence of sulphur in low amounts due to the unreacted calcium sulphate from PBW (Fig. 5 (C and E).

3.10 EGAs in civil engineering applications: A preliminary attempt

In order to target zero disposal, a preliminary attempt was made to evaluate the mechanical properties of a solidification material at the expense of exhausted EGAs along with PBW, FA and Ariake clay. The ratio of cement and water is quite significant to evaluate the mechanical properties of cement stabilized clay (Zhang et al., 2022). In continuation to our previous studies (Sugimoto et al., 2014; Li et al., 2018) and with a view towards stabilization of soft ground, the mechanical characteristics of solidification materials which includes EGA was found to be improved. Upon improving the FA quantity from 75 kg/cm^3 together with EGAs, the strength of compression of 210 kPa at the end of 7 days was measured up to 510 kPa after 28 days by witnessing the effect of materials solidification. The measured strength after the above curing periods was 4 to 10 times higher than that required for the improved construction of the bank body for agricultural irrigation in Saga plains. In line with the present addition of exhausted EGAs, it can be inferred that strong alkaline conditions (pH 10.5) release silica and alumina from EGAs and clay minerals that eventually react to form a new cementation products (Guney et al., 2017). It is further envisaged strongly to continue the present work on various civil engineering aspects in the near future.

3.11 Characterization studies

3.11.1 BET study

The nitrogen adsorption – desorption isotherms and the pore size distribution curves for the electro-generated aluminas (EGAs) are shown in Fig. 6 (A and B). The hysteresis loops indicated the formation of mesoporous alumina of H2 type by resembling the existence of ink – bottle like pores in EGAs (Jiao et al., 2012). The BET surface area of EGA (Al) and EGA (Fe) are 200.6 m^2g^{-1} and 274.7 m^2g^{-1} respectively. The surface area, pore volume and pore diameter for EGA (Fe) was greater than that of EGA (Al) as shown in Table – 6. The increase in the textural properties for EGA (Fe) witnessed the increased efficiency of fluoride and nitrate adsorption than EGA (Al). The range of pore diameter (d_p) appeared wider and corresponding change in the volume (dV/d_p) was found higher for EGA (Fe) than that of EGA (Al). The value of dV/d_p declines after the d_p value greater than 18 nm. As shown in Eq. (13), there is a relationship between surface area (S_a) and the total pore volume (V_p) and the average pore radius (r_p) where 'f' relies on the pore's geometry (Sanchez-Valente et al., 2003).

$$S_a = fV_p/r_p \quad \text{……. (13)}$$

Based on the above equation, the pore geometry of EGA (Fe) was greater than that of EGA (Al). The diminution of hysteresis from EGA (Al) to EGA (Fe) was observed with a decrease in the crystallite sizes (boehmite and bayerite) and an increase in their total pore volumes.

3.11.2 Field emission scanning electron microscopic (FESEM) study

The scanning electron micrographs of EGAs represented the heterogeneous and sharp edged large particles. A similar observation (Rajabi and Derakhshan, 2010) in which the existence of boehmite phases in the bulk of untransformed bayerite was reported. The formation of aggregated particles into large agglomerates is observed as shown in Fig. 7. The mass percentage of Al and O in EGAs according to EDS was in range of 33 – 34 and 66 – 67 respectively (Fig. 8). The obtained mass percentage data is closer to the average obtained from the Al and O mass percentage calculated from boehmite and bayerite phases and confirms the presence of the two phases. However, the mass of Al decreased by 2 – 3% with a change in the mass (%) of oxygen due to the newly bonded fluoride during adsorption. In conformity, the adsorbed fluoride onto EGAs was corroborated from the EDS analysis with the mass value in the range of 1.01 – 4.43%. The EGAs after the treatment of real time effluents (Fig. S5) was observed with fluoride (4.0±1.5 mass %) along with Al (36±2 mass %) and O (51±1 mass %). The present morphology of EGAs is similar to those prepared by Rajabi and Derakhshan (2010) at room temperature. The presence of Cl^- in EGAs (atomic

mass % = 0.77 – 2.09) without the presence of Na^+ leads to the suggestion of anion exchange between chloride and hydroxide anions (Tchomgui – Kamga et al., 2013) based on the Eq. (14) as shown below.

$$Al_2O_3 + X^{n-} \rightarrow Al_2O_3.(H_2O)_{X-n}.H_nX + nOH^-;\ X^{n-}\ is\ {SO_4}^{2-} or\ Cl^- \quad \ldots\ldots (14)$$

3.11.3 X – Ray diffraction study

The X – Ray diffraction patterns (Fig. 9) demonstrated the crystalline nature of EGAs distinguished with boehmite and bayerite phases. The crystalline form of boehmite in EGA (Al) was observed with the space group (Cmcm (63) with the unit cell parameters: a = 2.8130Å, b = 12.2343 Å, c = 3.7397 Å. However, the space group of boehmite differ in EGA (Fe) with Amam (63) for the unit cell parameters: a = 3.72 (2) Å, 12.44 (4) Å, c = 2.804 (8) Å. The crystallite size of boehmite was 34.1 (8) Å and 32.9 (6) Å for the synthesized EGAs from Al/Al and Al/Fe systems respectively (Bokhimi et al., 2001). The second crystalline phase was bayerite with the space group: 14:P121/a1, unique-b, cell3 for both EGAs. The size of the crystals for bayerite in EGAs obtained from Al/Al system (42 (5) Å was two times higher than that of Al/Fe system (21.5(10) Å for the unit cell parameters a = 5.08±0.03 Å, b = 8.68±0.02 Å and c = 4.68±0.03 Å. Similar crystallite size for boehmite was reported from the electro-synthesis of EGAs using ammonium salts (Tchomgui – Kamga et al., 2013). The appearance of peaks for boehmite is broad than that of bayerite which look thinner. In accordance with the earlier reports (Tchomgui – Kamga et al., 2013; Due et al., 2009), the formation of boehmite and bayerite occurs in more alkaline electrolytes (pH 8 – 10). In addition to boehmite, the strongly basic condition supports the transformation of boehmite to bayerite as shown in Eq. (15).

$$AlO(OH) + H_2O \rightarrow Al(OH)_3 \quad \ldots\ldots\ldots (15)$$

The XRD patterns of EGAs did not show any modifications after the treatment of synthetic solutions and the real time effluent samples.

3.11.4 X – Ray Photoelectron spectroscopic study

The intensity of photoelectron peaks plotted against the binding energy (eV) for EGAs are shown in Fig. 10 (A – E). The XPS line for aluminium (Al_{2p}) observed at the binding energy of 74.2 eV ensured the formations of Al $(OH)_3$ and AlO(OH) in EGAs (Jia et al., 2015; Lin et al., 2020). The peak (74.2 eV) that appears between the binding energies of Al – O

(aluminium oxide) and pseudo-boehmite (AlOOH) was referred by Lin et al., 2020. The peaks for the adsorbed fluoride (F_{1s}) onto EGAs at 684.4 eV and 687.8 eV were observed. The peaks of (Al) and O_{1s} at 76.7 eV and 531.8 eV corroborated the formation of fluoride substituted alumina, $AlF_2(OH)$ due to adsorption. Evidently, the shift in the peaks towards the lower binding energy from 531.9 eV to 531.8 eV inferred the substitution of fluorine in $AlO(OH)$ to form $AlF_2(OH)$. In view of substitution in alumina, Tago et al., (2017) reported the shift of binding energy in oxygen due to the nature of chemical bonds. The additional peaks at 534.7 eV (O_{1s}) and 76.7 eV ($Al\ 2p_{\frac{3}{2}}$) also inferred the formation of the fluoride substituted alumina during the adsorption process. The binding energy of 398.2 eV witnessed the adsorption of nitrate (Pashutski and Folman, 1989) onto EGAs as shown in the XPS spectra (Fig. 11C).

3.11.5 Fourier Transform Infrared spectroscopic study

The IR bands represented the boehmite form of EGAs around 855 cm^{-1} (υ_{as}), 745 cm^{-1} (υ_s), 618 cm^{-1} and 470 cm^{-1} (δ_s) attributing the Al – O bonds (Li et al., 2008). Furthermore, the symmetric and asymmetric deformation vibrations of Al – O – H modes appeared around 1065 cm^{-1} and 1639 cm^{-1} respectively (Ji et al., 2012). A shoulder peak around 1360 cm^{-1} attributed the adsorbed nitrate ions in EGAs as reported by Jia et al., 2015. The assignments between 3000 cm^{-1} and 3700 cm^{-1} attributed the hydroxyl stretching vibrations of the boehmite and bayerite forms. The bands around 3089 cm^{-1} and 3279 cm^{-1} corroborated the stretching of hydroxyl groups bonded to Al which remain unaffected after the adsorption of fluoride and nitrate (Fig. 10F). In particular, the bands at 855 cm^{-1}, 3452 cm^{-1}, 3547 cm^{-1} and 3662 cm^{-1} belong to the bayerite phase whereas the other bands correspond to the boehmite phase of EGAs (Rajabi and Derakhshan, 2010). The stretching vibrations are in accordance with the observations of Jiao et al., (2012) who attempted the synthesis of alumina from hydrates.

3.11.6 Thermo-gravimetric study

The TG – DTA studies of EGAs are shown in Fig. S6. The curves illustrated about 6% of mass loss at about 100°C due to desorption of water molecules in EGA (Al) and EGA (Fe) materials (Zaidi et al., 2019). Later, the mass losses up to 26% occurred at 470°C due to the dehydration of boehmite and bayerite phases of EGAs was in concordance with XRD patterns (Hanane et al., 2022). The plateau region was observed at 700°C after the total mass

loss of 28.5±0.5% in virgin EGAs. Based on the total loss of mass in EGAs and the mass loss in pure boehmite (15%) and bayerite (34.6%), the estimated percentage of boehmite and bayerite in EGAs are 49.6±0.3% and 50.4±0.3% respectively. The existence of the two phases in virgin EGAs is found in accordance with the observations from XRD and FTIR studies. On the other hand, the reduction (~3 – 4%) in the total mass loss was observed in EGAs after treatment with aqueous fluoride solution and real effluent samples. The reduced loss is associated with the formation of $AlO(F)$ and $AlF_2(OH)$ during the adsorption treatment which restricts the transformation of alumina by dehydration (Eq. 16 and Eq. 17) unlike the feasible conversion in boehmite (Eq. 18). The additional weight loss in EGAs after treatment with the mixture was 32.5±1.5% corroborated the decomposition of adsorbed nitrate onto EGAs (Peng et al., 2019).

$$AlO(OH) + F^- \rightarrow AlO(F) \quad \text{..... (16)}$$

$$AlO(OH) + 2F^- \rightarrow AlF_2(OH) \quad \text{..... (17)}$$

$$AlO(OH) \xrightarrow[450℃]{\Delta} Al_2O_3 \quad \text{..... (18)}$$

3.12 Proposed mechanism

The adsorptive removal of fluoride and nitrate can be predicted with the mechanism of electrostatic forces of attraction between the fluoride and nitrate and the protonated alumina as shown in Eq. (1) – (4). In support of the ion – exchange mechanism, the formation of $AlF_2(OH)$ and $AlO(F)$ the adsorption of fluoride was evident through XPS and TGA studies. Accordingly, the validation of pseudo – second – order (kinetic), Langmuir and DKR models was substantiated for the participation of chemical forces during the adsorption process. In the case of converting the recovered fluoride into fluorapatite using PBW, the following Eq. (19 – 20) is thus feasible.

$$10CaSO_4 0.5H_2O + 6(NH_4)_2HPO_4 \rightarrow Ca_{10}(PO_4)_6(OH)_2 + 6(NH_4)_2SO_4 + 4H_2SO_4 + 3H_2O \quad \text{..... (19)}$$

$$Ca_{10}(PO_4)_6(OH)_2 + 2F^- \rightarrow Ca_{10}(PO_4)_6F_2 + 2OH^- \quad \text{..... (20)}$$

3.13 Cost analysis

The cost of synthesizing EGAs includes the consumption of energy, electrode and chemicals. At first, the energy consumption (ENC) is calculated (Eq. 21) using the volume of the NaCl electrolyte (V) at an electric voltage (U) of the EC reactor with a current (I) for the time (t) of

the electrolysis process. For the synthesis of EGAs, the energy consumed during the electrolysis of 1 L of NaCl solution with a current of 0.8 A at a potential of 6.5 V for 1.5 h was 28.1 kwh.m^{-3}.

$$ENC = \left(\frac{KWh}{m^3}\right) = \frac{U.I.t}{V} = \frac{6.5 \times 0.8 \times (1.5 \times 60^2)}{1 \times 10^{-3}} = 28.1\ kwh.m^{-3} \quad \text{.....(21)}$$

On summing up the costs of energy consumption with electrode and sodium chloride consumptions, the cost for synthesizing one gram of EGA (Al) and EGA (Fe) was calculated to be 2.32 USD and 2.54 USD respectively. The calculation details are given in the Table S1. The cost reduction for EGAs is also accountable owing to regeneration of EGAs, one gram of EGA (Al) and EGA (Fe) can be estimated to be 0.464 USD and 0.508 USD respectively. Furthermore the reduction of cost is evident from the dual removal role of EGAs unlike the removal of individual ions. In accordance with the present context, Biswal et al., (2022) studied the synthesis cost for various metal – organic framework based adsorbents.

4. Conclusion

The synthesis of electro – generated alumina (EGA) using Al/Al and Al/Fe electrodes in sodium chloride medium demonstrated the presence of mesoporous (H2 type), crystalline phases of boehmite and bayerite as per the X – ray diffraction results. The adsorption rates of fluoride and nitrate during the first five minutes was quite high due to the dense protonated EGA sites albeit the adsorptive removal of fluoride (99.5±0.04%) was higher than that of nitrate (83±1%). The highest removal of fluoride and nitrate from the mixture was studied at pH 6.02±0.03 and pH 7.03±0.04 in compliance with the respective pH_{zpc} values of 7.6 and 8.3. The presence of nitrate in the fluoride/nitrate mixture did not affect the fluoride removal efficiency and conspicuously, the EGA (Al) had a better fluoride sorptive response profile than EGA (Fe). The adsorption was endothermic in nature and got influenced by temperature at different initial concentrations of fluoride and nitrate. The interference of sulphate was highly significant by inhibiting the sorption of nitrate (78 – 84%) onto both EGAs. The predominance of chemisorption was substantiated by pseudo – second – order (kinetic) and Langmuir (isotherm) models. The thermodynamic parameters inferred that the sorption was endothermic (positive ΔH^o) and spontaneous (negative ΔG^o) in nature. The application of both EGAs and their mixture was proved remarkable in a real wastewater containing 14 mg F^- and 67 mg NO_3^- per litre. In the fluoride/nitrate (1:1) mixture, the removal efficiency of fluoride and nitrate was quite consistent in the case of fluoride (99 – 80 %) than that of nitrate

(71 – 55%) after five regeneration cycles. The scope of converting the recovered fluoride into fluorapatite was made feasible using waste plaster board by hydrothermal treatment with diammonium hydrogen phosphate. The possible substitution of fluoride for hydroxyl groups in boehmite phases was substantiated by the XPS and TGA studies evidencing the formations of $AlO(F)$ and $AlF_2(OH)$. The formation of fluorapatite from the recovered fluoride was confirmed by the XRD, SEM (EDS) and FTIR studies. The exhausted EGA after the fifth regeneration cycle was utilized with ariake clay, plasterboard waste and cement for the purpose of construction applications.

Credit author statement

H. Tounsi : Investigation, **T. Chaabane :** Conceptualisation and methodology & Supervision, **K.Omine :** Supervision, **V. Sivasankar :** Writing Original Draft – Review and Editing, **H. Sano** and **M. Hecini :** Resources, **A. Darchen :** Writing – Review and Editing

Acknowledgements

We would like to thank the heads of the collaborating institute, namely Research Center in Semiconductor Technology for Energy (CRTSE, Algiers, Algeria), P.G. and Research Department of Chemistry of Pachaiyappa's College (Chennai, India), Nagasaki University (Japan), USTHB (Algiers, Algeria), CNRS and National College of Chemistry (ENSCR, Rennes, France). Mrs H. Tounsi deeply thanks the Director of CRTSE for giving her the opportunity to carry out research at Geo-technological Laboratory, Nagasaki University, Japan under the supervision of Prof. Kiyoshi Omine and the Ministry of Higher Education and Scientific Research, Algeria for the financing of her internship.

Declaration of competing interest

The authors declare that they have no known competing financial interests or personal relationships that could have appeared to influence the work reported in this paper.

Reference

Adu – Boahene, F., Boakye, P., Agyemang, F.O., Kanjua, J., Oduro – Kwarteng, S., 2023. Understanding fluoride adsorption from groundwater by alumina modified with alum using PHREEQC surface complexation model. Sci. Rep. 13, 12307. https://doi.org/10.1038/s41598-023-38564-1

Aliaskari, M., Schafer, A.I., 2021. Nitrate, arsenic and fluoride removal by electrodialysis from brackish groundwater. Wat. Res. 190 (15), 116683. https://doi.org/10.1016/j.watres.2020.116683

Allen, S.J., McCay, G., Khader, K.Y.H., 1989. Intraparticle diffusion of a basic dye during adsorption onto sphagnum peat. Environ. Pollut. 56, 39–50.

Aoudj, S., Drouiche, N., Hecini, M., Ouslimane, T., Palaouane, B., 2012. Coagulation as a post-treatment method for the defluoridation of photovoltaic cell manufacturing wastewater, Procedia Eng. 33, 111–120. http://dx.doi.org/10.1016/j.proeng.2012.01.1183

Arcibar – Orozco, J.A., Flores – Rojas, A.I., Rangal – Mendez, J.R., Diaz – Flores, P.E., 2018. Synergistic effect of zeolite/chitosan in the removal of fluoride from aqueous solution, Environ. Technol. https://doi.org/10.1080/09593330.2018/1542033

Ashoori, R., Samaei, M.R., Yousefinejad, S., Azhdarpoor, A., Emadi, Z., Mohammadpour, A., Lari, A.R., Khaneghah, A.M., 2022. Simultaneous removal of fluoride and nitrate from synthetic aqueous solution and groundwater by the electrochemical process using non – coated and coated anode electrodes: A human health risk study. Environ. Res. 214 (3), 113938. https://doi.org/10.1016/j.envres.2022.113938

Ayat, M., Belhousse, S., Boarino, L., Gabouse, N., Boukherroub, R., Kechouane, M., 2014. Formation of nanostructured silicon surfaces by stain etching. Nanoscale Res. Lett. 9, 482. https://doi.org/10.1186/1556-276x-9-482

Belkada, F.D., Kitous, O., Drouiche, N., Aoudj, S., Bouchelaghen, O., Abdi, N., Grib, H., Mameri, N., 2018. Electrodialysis for fluoride and nitrate removal from synthesized photovoltaic industry wastewater. Sep. Purif. Technol. 204, 108 – 115. https://doi.org/10.1016/j.seppur.2018.04.068

Bhatnagar, A., Kumar, E., Sillanpää, M., 2010. Nitrate removal from water by nanoalumina : Characterization and sorption studies, Chem. Eng. J. 163, 317–323, https://doi.org/10.1016/j.cej.2010.08.008

Billenkamp, E., 2011. Water and wastewater treatment for solar industry, Trade J. Water Wastewater Manage (Industrial Water Modern Methods), pp. 16–18.

Biswal, L., Goodwill, J.E., Jaiak, C., Chatterjee, S., 2022. Versatility, cost analysis, and scale – in fluoride and arsenic removal using metal – organic framework – based adsorbents. Sep. Purif. Technol. 51, 408 – 426. https://doi.org/10.1080/15422119.2021.1956539

Bokhimi, X., Toledo – Antonio, J.A., Guzmann – Castillo, M.L., Hernandez – Beltran, F., 2001. Relationship between crystallite size and bond lengths in boehmite. J. Solid State Chem. 159, 32 – 40. https://doi.org/10.1006/jssc.2001.9124

Chang, M.F., Liu, J.C., 2007. Precipitation removal of fluoride from semiconductor wastewater. J. Environ. Eng. 133 (4), 419 – 425. https://doi.org/10.10161/(ASCE)0733-9372(2007)133:4(419)

Chu, L., Zhang, C., Yu, J., Sun, X., Zhou, X., Zhang, Y., 2022. Adsorption of nitrate from interflow by the Mg/Fe Calcined layered double hydroxides. Wat. Sci. Technol. 86 (3), 511. https://doi.org/10.2166/wst.2022.224

de Paula, N., Maraschin, M., de Souza, D.M., Dotto, G.L., Jahn, S.L., dos Reis, G.S., Goncalves, J.O., Lima, E.C., Naushad, Mu., Carissimi, E., 2023. Application of ozone to enhance the defluoridation property of activated alumina: A novel approach. J. Environ. Chem. Eng. 11(5), 110384. https://doi.org/10.1016/j.jece.2023.110384

Diwani, G.El., Amin, K. Sh., Attia, N.K., Hawash, S.I., 2022. Fluoride pollutants removal from industrial wastewater. Bull. Natl. Res. Cent. 46, 143. https://doi.org/10.1186/s42269-022-00833

Drouiche, N., Djouadi-Belkada, F., Ouslimane, T., Kefaifi, A., Fathi, J., Ahmetovic, E., 2013. Photovoltaic solar cells industry wastewater treatment, Desalin. Water Treat. 51 (31 – 33), 5965 – 5973. http://dx.doi.org/10.1080/19443994.2012.763217

Du, X., Wang, Y., Su, X., Li, J., 2009. Influences of pH value on the microstructure and phase transformation of aluminium hydroxide. Powder Technol. 192, 40 – 46.

Dubinin, M.M., 1960. The potential theory of adsorption gases and vapors for adsorbents with energetically non-uniform surfaces. Chem. Rev. 60, 235–241.

Expert_Market_Research, Global industrial wastewater treatment trend by year. Expert Market Res. 2022. https://www.24chemicalresearch.com/download-sample/247298/global-industrial-wastewater-treatment-material-forecast-market-2023-2030-232

Freundlich, H.M.F., 1906. Over the adsorption in solution. J Phys Chem 57: 385–471.

Fritche, U. 1993. Removal of nitrates and other anions from water by yellow bismuth hydroxide. J. Environ. Sci. Health A 28 (9), 1903–1913.

Gai, W-Z., Zhang, S-H., Yang, Y., Zhang, ., Deng, Z-Y., 2021. Separation of excess fluoride from water using amorphous and crystalline AlOOH adsorbents. ACS Omega 6, 16488 – 16497. https://doi.org/10.1021/acsomega.1C01620

Gao, Y., You, K., Fu, J., Wang, J., Qian, W., 2022. Manganese modified activated alumina through impregnation for enhanced adsorption capacity of fluoride ions. Water 14 (17), 2673. https://doi.org/10.3390/w14172673

Gogoi, H., Leiviska, T., Ramo, J., Tanskanen, J., 2019. Production of animated peat from branched polethylenimine and glycidyltrimethylammonium chloride for sulphate removal from mining water. Environ. Res. 174, 323 – 334. https://doi.org/j.envres.2019.05.022

Gopal, V., Elango, K.P., 2007. Equilibrium, kinetic and thermodynamic studies of adsorption of fluoride onto plaster of paris. J. Hazard. Mater. 141 (1) 98 – 105. https://doi.org/j.jhazmat.2006.06.099

Guan, C., Xu, Z., Zhu, H., Lv, X., Liu, Q., 2022. Insights into the mechanism of fluoride adsorption over different crystal phase alumina surfaces. J. Hazard. Mater. 423, 127109. https://doi.org/10.1016/j.jhazmat.2021.127109

Guney, O.C., Firoozi, A.A., Baghini, M.S., 2017. Fundamentals of soil stabilization. Geo – Eng. 8, 26. https://doi.org/10.1186/s40703-017-0064-9

He, Y., Zhang, L., An, X., Wan, G., Zhu, W., Luo, Y., 2019. Enhanced fluoride removal from water by rare earth (La and Ce) modified alumina: Adsorption isotherms, kinetics, thermodynamics and mechanism. Sci. Total Environ. 688, 184 – 198. https://doi.org/10.1016/j.scitotenv.2019.06.175

He, H., Huang, Y., Yan, M., Xie, Y., Li, Y., 2020. Synergistic effect of electrostatic adsorption and ion exchange for efficient removal of nitrate, Colloids Surfaces A Physicochem. Eng. Asp. 584, 123973. https://doi.org/10.1016/j.colsurfa.2019.123973

Ho, Y.S., McKay, G., 1998. Sorption of dye from aqueous solution by peat. Chem Eng J 70, 115–124.

Ho, Y.S., 2006. Second-order-kinetic model for the sorption of cadmium onto tree fern: a comparison of linear and non-linear methods. Water Res. 40, 119–125.

Ho, J-S., Takahashi, M., Iizuka, A., 2023. Simultaneously removal of fluoride and phosphate from semiconductor wastewater via chemical precipitation of calcium fluoride and hydroxyapatite using by-product of recycled aggregate. Chemosphere 340, 139875. https://doi.org/10.1016/j.chemosphere.2023.139875

Hosni, K., Srasra, E., 2008. Nitrate adsorption from aqueous solution by M^{II} – Al – CO3 layered double hydroxide. Inorg. Mater. 44(7) 742 – 749. https://doi.org/10.1134/S0020168508070121

Huang, L., Yang, Z., He, Y., Chai, L., Yang, W., Deng, H., Wang, H., Chen, Y., Crittenden, J., 2020. Adsorption mechanism for removing different species of fluoride by designing of core – shell boehmite. J. Hazard. Mater. 394, 122555. https://doi.org/10.1016/j.jhazmat.2020.122555

Huang, S., Hu, M., Li, D., Wang, L., Zhang, C., Li, K., He, Q., 2020. Fluoride sorption from aqueous solution using Al(OH)3 – modified hydroxyapatite nanosheet. Fuel 279, 118486. https://doi.org/10.1016/j.fuel.2020.118486

Innocenzi, V., Zueva, S. B., Veglio, F., Michelis, I.D., 2021. Pilot-scale experiences with aerobic treatment and chemical proceses of industrial wastewaters from electronics and semiconductor industry. Energies 14, 5340. https://doi.org/10.3390/en14175340

Jeong, J.-Y., Song, Y.-H., Kim, J.-H., & Park, J.-Y. 2013. Simultaneous removal of nitrate, phosphate, and fluoride using a ZVI-packed bed electrolytic cell. Desalin. Water Treat. 52(4-6), 737–743. https://doi.org/10.1080/19443994.2013.827321

Ji, G., Li, M., Li, G., Gao, G., Zou, H., Gan, S., Xu, X., 2012. Hydrothermal synthesis of hierarchical micron flower – like ϒ - AlOOH and ϒ – Al_2O_3 superstructures from oil shale ash. Powder Technol. 215 – 216, 54 – 58. https://doi.org/10.1016/j.powtech.2011.09.005

Jia, Y., Zhu, B-S., Jin, Z., Sun, B., Tao, L., Yu, X.Y., Kong, L-T., 2015. Fluoride removal mechanism of bayerite/boehmite nanocomposites: Roles of surface hydroxyl groups and

the nitrate anions. J. Colloid. Interf. Sci. 440, 60 – 67. https://dx.doi.org/10.1016/j.jcis2014.10.069

Jiao, W.Q., Yue, M.B., Wang, Y.M., He, M-Y., 2012. Synthesis of morphology – controlled mesoporous transition aluminas derived from the decomposition of hydrates. Micropor. Mesopor. Mater. 147, 167 – 177. https://doi.org/10.1016/j.micromeso.2011.06.012

John, Y., David, V.E., Mmereki, D., 2018. A Comparative Study on Removal of Hazardous Anions from Water by Adsorption: A Review. Int. J. Chem. Eng. Article ID: 3975948. https://doi.org/10.1155/2018/3975948

Karimi, Z., Rahbar – Kelishami, A., 2022. Preparation of highly efficient and eco-friendly alumina magnetic hybrid nanosorbent from red mud: Excellent adsorption capacity towards nitrate. J. Mol. Liq. 368, 120751. https://doi.org/10.1016/j.molliq.2022.120751

Kassahun, F., Taddesse, A.M., Teju, E., Bogale, Y., 2023. Magnetic $Al_2O_3/ZrO_2/Fe_3O_4$ nanocomposite: Synthesis, characterization and application for the adsorptive removal of nitrate from aqueous solution. Groundw. Sustain. Dev. 20, 100873. https://doi.org/10.1016/j.gsd.2022.100873

Katheresan, V., Kansedo, J., Lau, S.Y., 2018. Efficiency of various recent wastewater dye removal methods: A review. J. Environ. Chem. Eng. 6, 4676 – 4697. https://doi.org/10.1016/j.jece.2018.06.060

Khatamian, M., Derakhshan, S.K., Nami, S.H. *et al.* Nitrate removal study of synthesized nano γ-alumina and magnetite-alumina nanocomposite adsorbents prepared by various methods and precursors. *Sci Rep* **14**, 7673 (2024). https://doi.org/10.1038/s41598-024-58459-z

Kim, W-T., Lee, J-W., An, H-E., Cho, S-H., Jeong, S., 2023. Efficient fluoride wastewater treatment using eco-friendly synthesized AlOOH. Nanomater. 13, 2838. https://doi.org/10.3393/nano13212838

Kumari, R., Kumar, A., Sarkar, S., Ghosh, T.K., Basu, S., 2023. Zirconium fumarate metal – organic framework: a selective adsorbent for fluoride from industrial wastewater. Water Practise Technol. 18 (5) 1074. https://doi.org/10.2166/wpt.2023.066

Lagergren, S., 1898. Zur theorie der sogenannten adsorption geloster stoffe. Vet Akad Handl 24: 1–39.

Langmuir, I., 1918. The adsorption of gases on plane surfaces of glass, mica and platinum. J Am Chem Soc 40: 1361–1403.

Li, D.Y., Lin, Y.S., Li, Y.C., Shieh, D.L., Lin, J.L., 2008. Synthesis of mesoporous pseudoboehmite and alumina template with 1-hexadecyl-2,3,-dimethyl-imidazolium chloride. Micropor Mesopor Mat 108:276–282. https://doi.org/10.1016/j.micromeso.2007.04.009

Li, C., Shih, K., Gao, Y., Li, F., Wei, L., 2012. Dechlorinating transformation of propachlor through nucleophilic substitution by dithionate on the surface of alumina. J. Soils

Sediments 12, 724 – 733. https://doi.org/10.1007/s11368-012-0506–0

Li, J., Li, M., Yang, X., Zhang, Y., Liu, X., Liu, F., Meng, F., 2019. Morphology controlled synthesis of boehmite with enhanced efficiency for the removal of aqueous Cr (VI) and nitrates. Nanotechnol. 30, 195702. https://doi.org/10.1088/1361-6528/aaff21

Li, Y., Yang, Y., Qu, G., Ren, Y., Wang, Z., Ning, P., Wu, F., Chen, X., 2022. Reuse of secondary aluminium ash: Study on removal of fluoride from industrial wastewater by mesoporous alumina modified with citric acid. Environ. Technol. Inno. https://doi.org/10.1016/j.eti.2022.102868

Lin, J-Y., Chen, Y-L., Hong, X-Y., Huang, C., Huang, C.P., 2020. The role of fluoroaluminate complexes on the adsorption of fluoride onto hydrous alumina in aqueous solutions. J. Colloid. Interface Sci. 561, 275 – 286.

Maity, J.P., Hsu, C.M., Lin, T.J., Lee, W.C., Bhattacharya, P., Bundschuh, J., Chen, C.Y., 2018. Removal of fluoride from water through bacterial-surfactin mediated novel hydroxyapatite nanoparticle and its efficiency assessment: adsorption isotherm, adsorption kinetic and adsorption thermodynamics. Environ. Nanotechnol. Monit. Manag. 9, 18–28.

Mall, I.D., Srivastava, V.C., Kumar, G.V.A., Mishra, I.M., 2006. Characterization and utilization of mesoporous fertilizer plant waste carbon for adsorptive removal of dyes from aqueous solution. Colloids Surf. A 278, 175–187.

Mahinroosta, M., Allahverdi, A., 2021. Pilot-scale valorization of hazardous aluminium dross into γ-Al_2O_3 nanoadsorbent for efficient removal of fluoride, Environ. Technol. Innov. 23, 101549. https://doi.org/10.1016/j.eti.2021.101549

Onitsuka, K., Modmoltin, C., Kouno, M., 2001. Investigation on microstructure and strength of lime and cement stabilized Ariake clay. Reports on the Faculty of Science and Engineering, Saga, pp. 49 – 63. http://id.nii.ac.jp/1730/00018871

Oulebsir, A., Chaabane, T., Zaidi, S., Omine, K., Alonzo, V, Darchen, A., Msagati, T.A.M., Sivasankar, V., 2020. Preparation of mesoporous alumina electro-generated by electrocoagulation in NaCl electrolyte and application in fluoride removal with consistent regenerations. Arab. J. Chem. 13 (1) 271 – 289. https://doi.org/10.1016/j.arabjc.2017.04.007

Jalil, S.N.A., Amri, N., Ajien, A.A., Ismail, N.F., Ballinger, B., 2019. A hybrid electrocoagulation – adsorption process for fluoride removal from semi conductor wastewater. J. Phys.: Conf. Ser. 1349 012056. https://iopscience.iop.org/article/10.1088/1742-6596/1349/1/012056

Pashutski, A., Folman, M., 1989. Low temperature XPS studies of NO and N_2O adsorption on Al (100). Surf. Sci. 216, 395 – 408. https://doi.org/10.1016/0039-6028(89)90383-x

Pei, Y., Cheng, W., Liu, R., Di, H., Jiang, Y., Zheng, C., Jiang, Z., 2024. Synergistic effect and mechanism of nZVI/LDH composites adsorption coupled reduction of nitrate in micro – polluted water. J. Hazard. Mater. 464, 133023. https://doi.org/10.1016/j.jhazmat.2023.133023

Peng, C., Liu, F., Wang, Z., Wilson, B.P., Lundstrom, M., 2019. Selective extraction of lithium (Li) and preparation of battery grade lithium carbonate (Li_2CO_3) from spent Li – ion batteries in nitrate system. J. Power Sources 415, 179 – 188. https://doi.org/10.1016/j.jpowsour.2019.01.072

Park, J.Y., Byan, H-J., Choi, W-H., Kang, W-H., 2008. Cement paste column for simultaneous removal of fluoride, phosphate, and nitrate in acidic wastewater. Chemosphere 70(8), 1429 – 1437. https://doi.org/10.1016/j.chemosphere.2007.09.012

Pirasaheb, M., Mohammadi, H., Sharafi, K., Asadi, A., 2018. Fluoride and nitrate adsorption from water by Fe (III) – doped scoria: Optimising using response surface modelling, kinetic and equilibrium study. Wat. Sci. Technol: Water Supply, 18 (3), 1117 – 1132. https://doi.org/10.2166/ws.2017.185

Qiu, Y., Ren, L-F., Xia, L., Shao, J., Zhao, Y., Van der Bruggen, B., 2022. Investigation of fluoride and silica removal from semiconductor wastewaters with a clean coagulation – ultrafiltration process. Chem. Eng. J. 438, 135562. https://doi.org/10.1016/j.cej.2022.135562

Raj, S.K., Sharma, V., Yadav, A., Indurkar, P.D., Kulshrestha, V., 2023. Nano – alumina wraped carbon microspheres for ultra-high elimination of pentavalent arsenic and fluoride from potable water. J. Ind. Eng. Chem. 117, 402 – 413. https://doi.org/10.1016/j.jiec.2022.10.028

Rajabi, L., Derakhshan, A.A., 2010. Room temperature synthesis of Boehmite and crystallization of nanoparticles: Effect of concentration and ultrasound. Sci. Adv. Mater. 2, 163 – 172. https://doi.org/10.1166/sam.2010.1063

Rajkumar, S., Murugesh, S., Sivasankar, V., Darchen, A., Msagati, T.A.M., Chaabane, T., 2009. Low – cost fluoride adsorbents prepared from a renewable biowaste: Syntheses, characterization and modelling studies. Arab. J. Chem. 12 (8) 3004 – 3017. https://doi.org/10.1016/j.arabjc.2015.06.028

Ranjan, M., Singh, P. K. (2020). Concurrent removal of nitrate, fluoride and arsenic by mixed hydrous bismuth oxide from water. J. Water Supply: Res. Technol.-AQUA, 69 (5) 478 – 499. https://doi.org/10.2166/aqua.2020.026

Sanchez-Valente, J., Bokhimi, X., Hernandez, F., 2003. Physicochemical and Catalytic Properties of Sol-Gel Aluminas Aged under Hydrothermal Conditions. Langmuir 19, 3583–3588.

Sano, H., 2008. Reports of the faculty of engineering. Nagasaki Univ. 38 (70), 44–54.

Schick, P. Caullet, J. Paillaud, J. Patarin, C. Mangold-callarec, Microporous and Mesoporous Materials Batch-wise nitrate removal from water on a surfactantmodified zeolite, Micropor. Mesopor. Mater. 132 (2010) 395–400. https://doi.org/10.1016/j.micromeso.2010.03.018

Schmid, T., Jungnickel, R., Dariz, P., 2020. Insights into the $CaSO_4$ – H_2O system: A Raman

spectroscopic study. Minerals 10: 115.

Shen, C-W., Tran, P.P., Ly, P.T.M., 2018. Chemical waste management in the U.S. Semiconductor industry. Sustainability 10 (5), 1545. https://doi.org/10.3390/su10051545

Sim, J., Lee, J., Rho, H., Park, K-D., Choi, Y., Kim, D., Kim, H., Woo, Y.C., 2023. A review of semiconductor wastewater treatment processes: Current status, challenges and future trends. J. Clean. Prod. 429, 139570. https://doi.org/10.1016/j.j.clepro.2023.139570

Sivasankar, V., Omine, K., Sugimoto, S., Liu, K., 2018. Evaluation of fluoride in tank leaching test samples using Ariake Clay – Recycle Plaster mixed waste material specimens. 17th Global Joint Seminar on Geo – Environmental Engineering (GEE 2018), 25 and 26 May 2018, Fukuoka University, Fukuoka, Japan.

Sivasankar, V., Omine, K., Zhang, Z., Shi, S., Sano, H., Chicas, S.D., 2023. Plaster board waste (PBW) – A potential fluoride leaching source in soil/water environments and, fluoride immobilization studies using soils. Environ Res 218: 115005.

Su, J-f., Wu, Z-z., Huang, T-l, Zhang, H., Li, J-w., 2020. A new technology for simultaneous calcium – nitrate and fluoride removal in the biofilm reactor. J. Hazard. Mater. 399, 122846. https://doi.org/10.1016/j.jhazmat.2020.122846

Sugimoto, S., Omine, K., Jiang, Y., 2014. Effects of ground improvement on low alkaline stabilizer with recycled plaster. 9th International Symposium on Lowland Technology, September 29 – October 1, 2014, Saga, Japan.

Tao, W., Zhong, H., Pan, X., Wang, P., Wang, H., Huang, L., 2020. Removal of fluoride from wastewater solution using Ce-AlOOH with oxalic acid as modification. J. Hazard. Mater. **384**, 121373–121383. https://doi.org/10.1016/j.hazmat.2019.121373

Tago, T., Kataoka, N., Tanaka, H., Kinoshita, K., Kishida, S., 2017. XPS study from a clean surface of Al_2O_3 single crystals. Procedia Eng. 216, 175 – 181. https://doi.org/10.1016/j.proeng.2018.02.081

Tchomgui – Kamga, E., Audebrand, N., Darchen, A., (2013). Effect of co – existing ions during the preparation of alumina by electrolysis with aluminium soluble electrodes: Structure and defluoridation activity of electro-synthesized adsorbents. J. Hazard. Mater. 254 – 255, 125 – 133. https://doi.org/10.1016/j.jhazmat.2013.03.044

Teow, Y.H., Chiah, Y.H., Ho, K.C., Mahmoudi, E., 2022. Treatment of semiconductor industry wastewater with the application of ceramic membrane and polymeric membrane. J. Clean. Prod. 337, 130569. https://doi.org/10.1016/j.jclepro.2022.130569

Tie, J.X., Sang, S., Shang, Z.Y., Li, Y.Q., Xu, Z.T., Lian, M.L., Du, C.B., 2022. Preparation of Al – loaded magnetic Chinese medicine residue – derived biochar and application of it in fluoride removal. Ind. Crop. Prod. 184, 115037. https://doi.org/10.1016/j.indcrop.2022.115037

Tounsi, H., Chaabane, T., Omine, K., Sivasankar, V., Sano, H., Hecini, M., 2022. Electrocoagulation in the dual application on the simultaneous removal of fluoride and

nitrate anions through respective adsorption/reduction processes and modelling of continuous process. J. Water Process Eng. 46, 102584. https://doi.org/10.1016/j.jwpe.2022.102584

Turki, T., Hamdouni, A., Enesca, A., 2023. Fluoride adsorption from aqueous solution by modified zeolite – Kinetic and Isotherm studies. Molecules 28 (10), 4076. https://doi.org/10.3390/molecules28104076

Weber, W.J., Morris, J.C., 1963. Kinetics of adsorption on carbon from solution. J. Sanit. Eng. Div. Am. Soc. Civ. Eng. 89, 31–60.

Wu, K., Li, Y., Liu, T., Huang, Q., Yang, S., Wang, W., Jin, P., 2019. The simultaneous adsorption of nitrate and phosphate by an organic modified aluminium – manganese bimetal oxide: Adsorption properties and mechanisms. Appl. Surf. Sci. 478, 539 – 551. https://doi.org/10.1016/j.ap.susc.2019.01.194

Yang, K., Li, Y., Zhao, Z., Tian, Z., Lai, Y., 2020. Amorphous porous layered – Al_2O_3 derived from AlFuMOFs as an adsorbent for removing fluoride ions in industrial $ZnSO_4$ solution [J]. Chem. Eng. Res. Des. 153, 562 – 571. https://doi.org/10.1016/j.cherd.2019.11.019

Yang, K., Li, H., Lin, W., Chen, Z., Peng, S., Yu, K., Fang, Z., 2024. Performance and mechanism of hierarchical porous – Al_2O_3 – MgO nano sheets for removing fluoride ions from industrial $ZnSO_4$ solution. Sep. Purif. Technol. 330, 125255. https://doi.org.10.1016.j.seppur.2023.125255

You, H., Li, W., Zhang, Y., Meng, Z., Shang, Z., Feng, X., Ma, Y., Lu, J., Li, M., Niu, X., 2019. Enhanced removal of NO_3 – N from water using Fe – Al modified biochar: behaviour and mechanism. Wat. Sci. Technol. 80 (10) 2003 – 2012. https://doi.org/10.2166/wst.2020.033

Yu, C., Liu, L., Wang, X., Fu, J., Wu, Y., Feng, C., Wu, Y., Shen, J., 2023. Fluoride removal performance by highly porous activated alumina. J. Sol – Gel Sci. Technol. 106, 471 – 479. https://doi.org/10.1007/s10971-022-05722-2

Zaidi, S., Sivasankar, V., Chaabane, T., Alonzo, V., Omine, K., Maachi, R., Darchen, A., 2019. Preparation and characterizations of thermally regenerable electro-generated adsorbents (EGAs) for a competitor electrocoagulation process. J. Taiwan Inst. Chem. Eng. 97, 272 – 279. https://doi.org/10.1016/j.jtice.2019.02.009

Zhange, Z., Omine, K., Flemmy, S.O., Li, C., 2022. The liquid limit as a factor in assessing the improvement of stabilized cement – based highwater content clayey sediments. Materials 15, 7240. https://doi.org/10.3390/ma15207240

Zheng, T.-T., Sun, Z.-X., Yang, X-F., Yang, A., 2012. Sorption of phosphate onto mesoporous c-alumina studied with in-situ ATR-FTIR spectroscopy. Chem. Cent. J. 6, 419. https://doi.org/10.1186/1752-153X-6-26

Table – 1 Validation of kinetic models with the adsorption system of fluoride and nitrate from the binary fluoride/nitrate mixture

	EGA (Al)		EGA (Fe)	
Parameters	Fluoride	Nitrate	Fluoride	Nitrate
Pseudo - first - order				
$k_1 \times 10^{-2}$	4.88	2.62	2.44	2.53
q_e	4.459	1.315	4.180	1.355
R^2	0.880	0.877	0.945	0.864
Pseudo - second - order				
$k_1 \times 10^{-2}$	0.336*	1.00	0.348*	0.402
q_e	9.862	68.027	9.97	75.758
R^2	1.00	0.999	1.00	0.999
Intra-particle diffusion				
$k_{id} \times 10^{-2}$	5.78	2.22*	3.56	4.39*
C_1	9.407	51.17	9.69	41.70
R^2	0.906	0.970	0.936	0.966

* No exponential values obtained

Table – 2 Validation of isotherm models for the adsorption system of nitrate from the binary fluoride/nitrate mixture

Langmuir						
	Q^o		$b \times 10^{-3}$		R^2	
T (°C)	**EGA (Al)**	**EGA (Fe)**	**EGA (Al)**	**EGA (Fe)**	**EGA (Al)**	**EGA (Fe)**
15	112.3	135.1	3.19	3.55	0.967	0.987
25	136.9	163.9	3.82	3.89	0.977	0.980
35	196.1	222.2	2.93	3.08	0.943	0.984
45	200.0	232.6	3.40	3.20	0.947	0.973
Freundlich						
	K_F		n		R^2	
15	1.58	2.39	1.65	1.74	0.914	0.930
25	2.52	3.08	1.74	1.75	0.912	0.921
35	1.97	2.89	1.52	1.62	0.898	0.945
45	2.59	1.87	1.60	1.60	0.902	0.930
DKR						
	Q_m		E		R^2	
15	72.67	88.27	18.25	19.61	0.961	0.952
25	92.51	108.37	20.41	22.36	0.958	0.944
35	118.70	129.79	20.42	23.57	0.928	0.923
45	126.52	139.25	22.36	23.56	0.932	0.931

Table – 3 Validation of isotherm models for the adsorption system of fluoride from the binary fluoride/nitrate mixture

Langmuir						
	Q^o		$b \times 10^{-3}$		R^2	
T (°C)	**EGA (Al)**	**EGA (Fe)**	**EGA (Al)**	**EGA (Fe)**	**EGA (Al)**	**EGA (Fe)**
15	285.71	384.61	3.91	6.26	0.966	0.992
25	400.13	476.22	7.84	6.65	0.994	0.987
35	416.31	555.59	8.29	7.59	0.999	0.986
45	454.51	625.07	9.11	7.87	0.997	0.977
Freundlich						
	K_F		**n**		R^2	
15	8.58	13.13	1.82	1.99	0.988	0.944
25	12.58	15.45	1.95	1.93	0.956	0.950
35	15.77	18.93	1.99	1.92	0.945	0.945
45	20.91	19.35	2.11	1.86	0.971	0.959
DKR						
	Q_m		**E**		R^2	
15	216.3	249.4	40.82	21.32	0.851	0.927
25	246.1	297.1	50.01	22.37	0.906	0.908
35	274.1	336.8	70.92	23.58	0.910	0.901
45	292.0	341.1	79.05	24.25	0.868	0.890

Table – 4 Thermodynamic parameters for the simultaneous adsorption of fluoride and nitrate from the binary fluoride/nitrate mixture

	Temperature												
	288 K			298 K			308 K			318 K			
Adsorbent	ΔS^0	ΔH^0	ΔG^0	ΔS^0	ΔH^0	ΔG^0	ΔS^0	ΔH^0	ΔG^0	ΔS^0	ΔH^0	ΔG^0	E_a
Nitrate adsorption system													
EGA (Al)	95.9	24.50	- 3.18	101.2	26.90	- 3.25	79.6	20.98	- 3.53	86.60	23.38	- 4.17	19.6
EGA (Fe)	101.5	26.86	- 2.69	100.8	27.32	- 2.72	90.0	24.53	- 3.18	87.31	23.93	- 3.83	20.1
Fluoride adsorption system													
EGA (Al)	109.9	32.74	- 0.636	130.7	37.49	- 1.46	138.1	39.63	- 2.87	186.6	23.38	- 4.17	17.4
EGA (Fe)	135.8	38.44	- 0.671	134.2	38.51	- 1.48	136.2	39.89	- 2.07	154.2	25.46	- 3.57	18.2

ΔS^0 *is measured in* $Jmol^{-1}$; ΔH^0 *and* ΔG^0 *are measured in* $kJ(mol.K)^{-1}$; $R = 8.314\ J(mol.K)^{-1}$; E_a *in* $kJ\ mol^{-1}$

Table -5 Concentration dynamics of the other parameters in the untreated and treated effluents by adsorption process using EGAs

Dissolved ions	In Raw Effluent			In Treated Effluent
	E – 1	E – 2	E – 3	Range
pH	6.2	7.6	7.7	5.6 – 6.6
Al	BDL	BDL	BDL	BDL
Ca	0.84	1.75	0.85	0.56 – 0.78
Cr	BDL	BDL	BDL	BDL
Cu	0.005	0.003	0.005	0.001 – 0.004
Fe	0.001	0.012	0.004	BDL – 0.005
K	0.62	0.89	0.92	0.48 – 1.65
Mg	0.25	0.22	0.25	0.2 – 0.37
Na	132.2	1087.5	381.7	13.2 – 341.1
P	0.04	0.018	0.003	BDL – 0.19
Pb	0.009	0.005	0.006	0.004 – 0.06
Si	4.55	26.18	11.1	0.05 – 0.76

BDL – Below Detectable Level

Table – 6 Textural properties of EGAs

Physical properties	**EGA (Al)**	**EGA (Fe)**
Mean pore volume (cm^3g^{-1})	46.093	63.109
BET surface area (m^2g^{-1})	200.62	274.68
Total pore volume (cm^3g^{-1})	0.2023	0.3579
Pore volume (cm^3g^{-1})	0.2116	0.3577
Mean pore diameter (nm)	4.033	5.2122
Pore diameter (nm)	1.0454	1.3243
Average pore diameter (nm)	3.1495	4.2508
Middle pore diameter (nm)	3.8617	5.3548
Specific surface area (m^2g^{-1})	268.80	336.63
pH_{zpc}	7.6	8.3

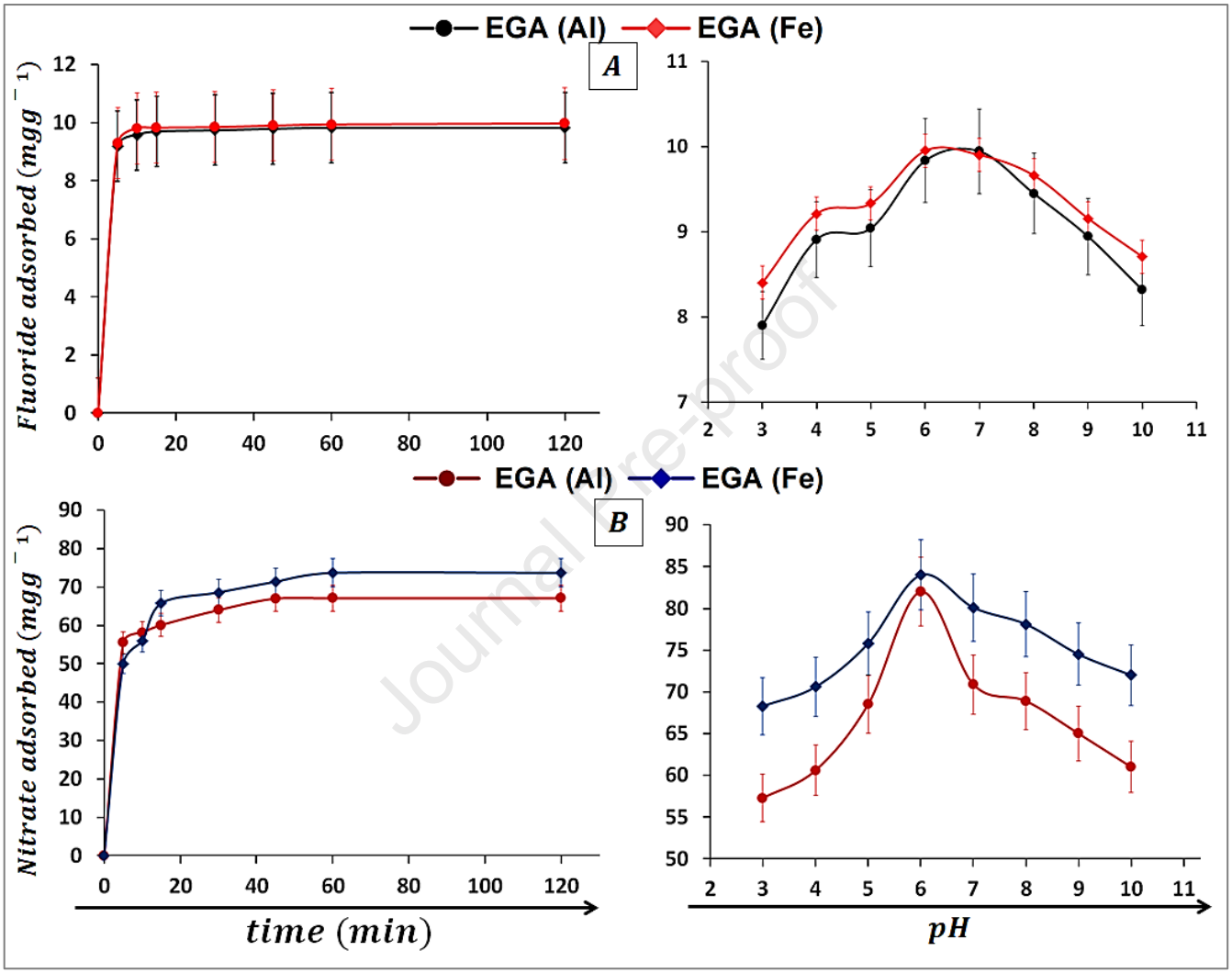

Fig. 1 Effect of time and pH on the adsorption of fluoride (A) nitrate (B) in the fluoride/nitrate binary mixture

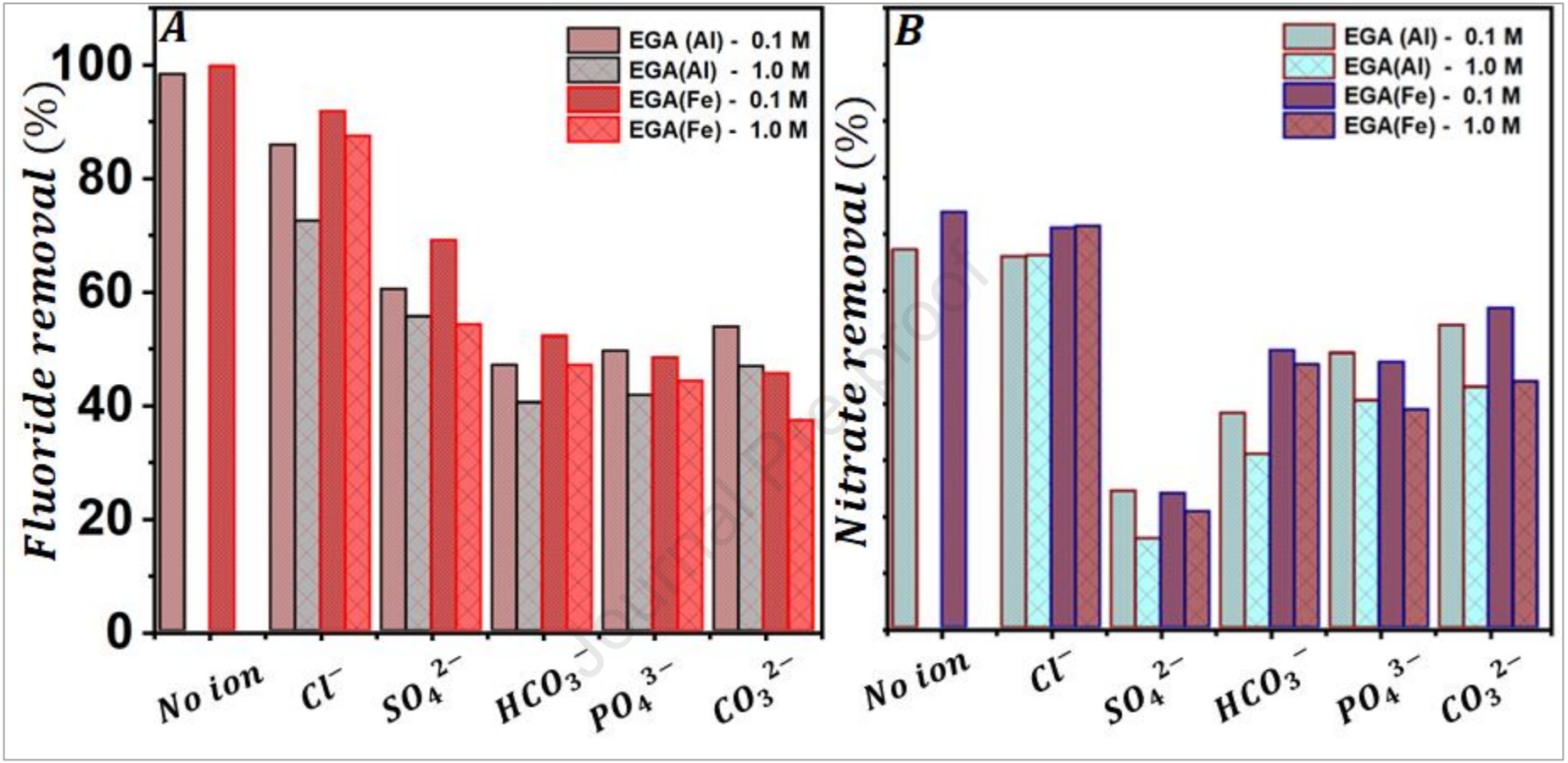

Fig. 2 Interference of accompanying ions in fluoride (A) and nitrate (B) removal from the fluoride/nitrate binary mixture

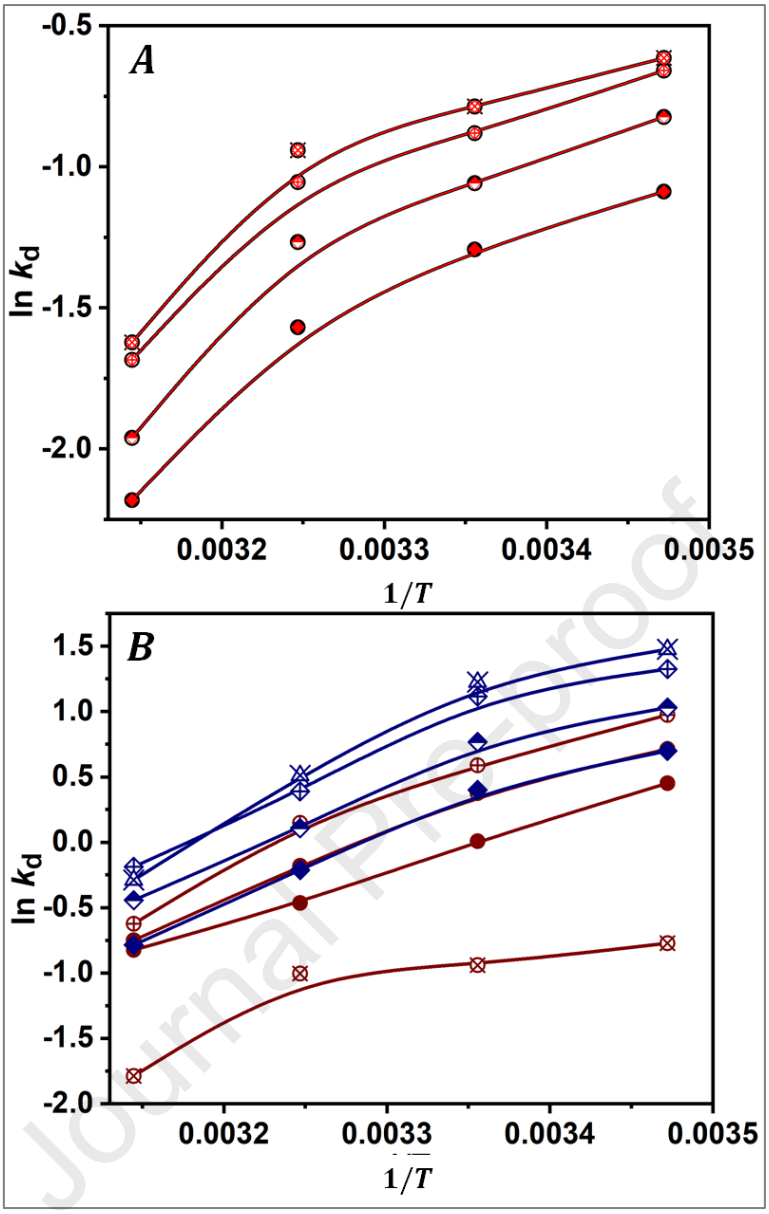

Fig. 3 Plot of ln k_d versus 1/T for the determination of thermodynamic parameters for the adsorption of fluoride (A) and nitrate (B) in the fluoride/nitrate binary mixture

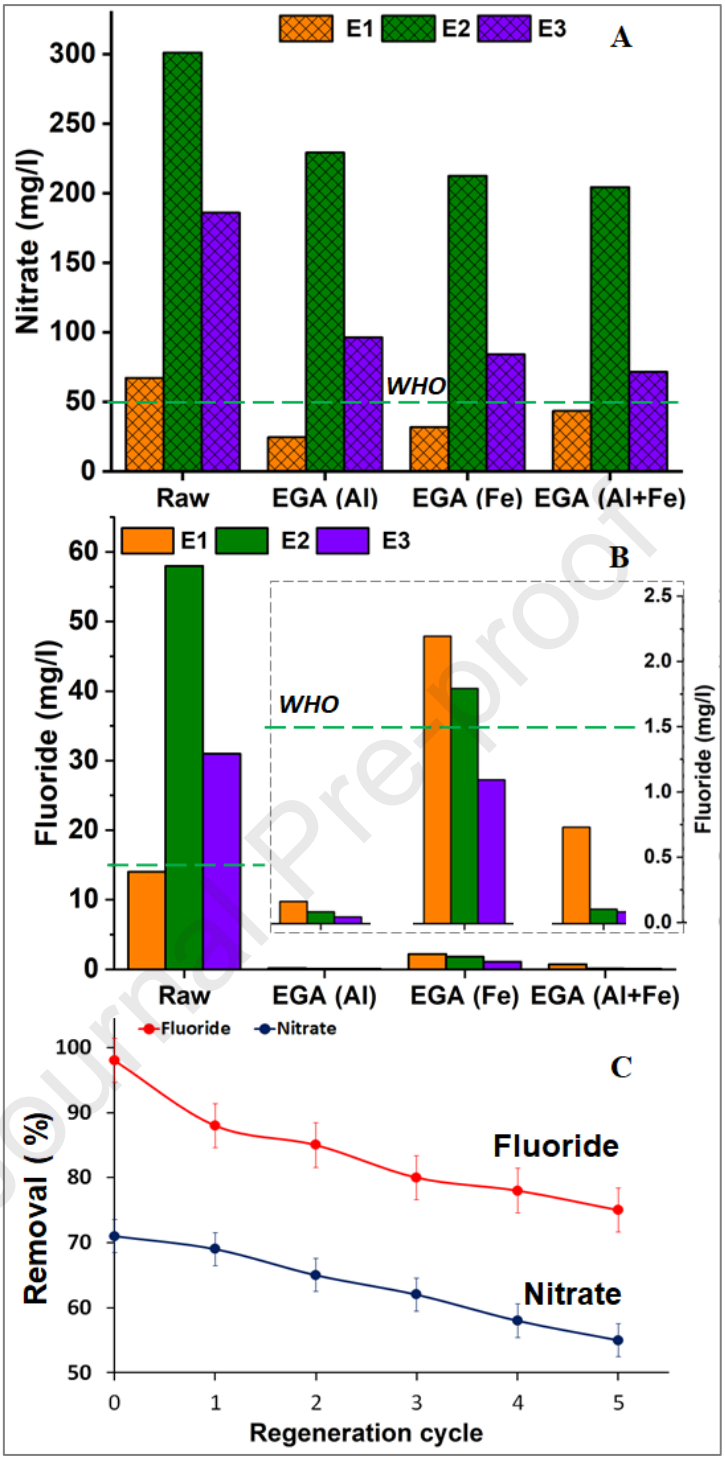

Fig. 4 Fluoride and nitrate concentrations in the treated effluents using EGAs

Conditions:

For A and B:

Initial F^- concentrations: [E1] = 14 mg L^{-1}; [E2] = 58 mgL^{-1}; [E3] = 31 mgL^{-1}

Initial NO_3^- concentrations: [E1] = 67 mgL^{-1}; [E2] = 301 mgL^{-1}; [E3] = 186 mgL^{-1}

For C: *Initial F^- concentration = Initial NO_3^- concentration = 50 mg L^{-1}; pH = 6.25±0.05; contact time = 60 min; [NaOH] = 0.1 M; Adsorbent dose = 1 g of EGA mixture, 0.5 g EGA (Al) + 0.5 g EGA (Fe)*

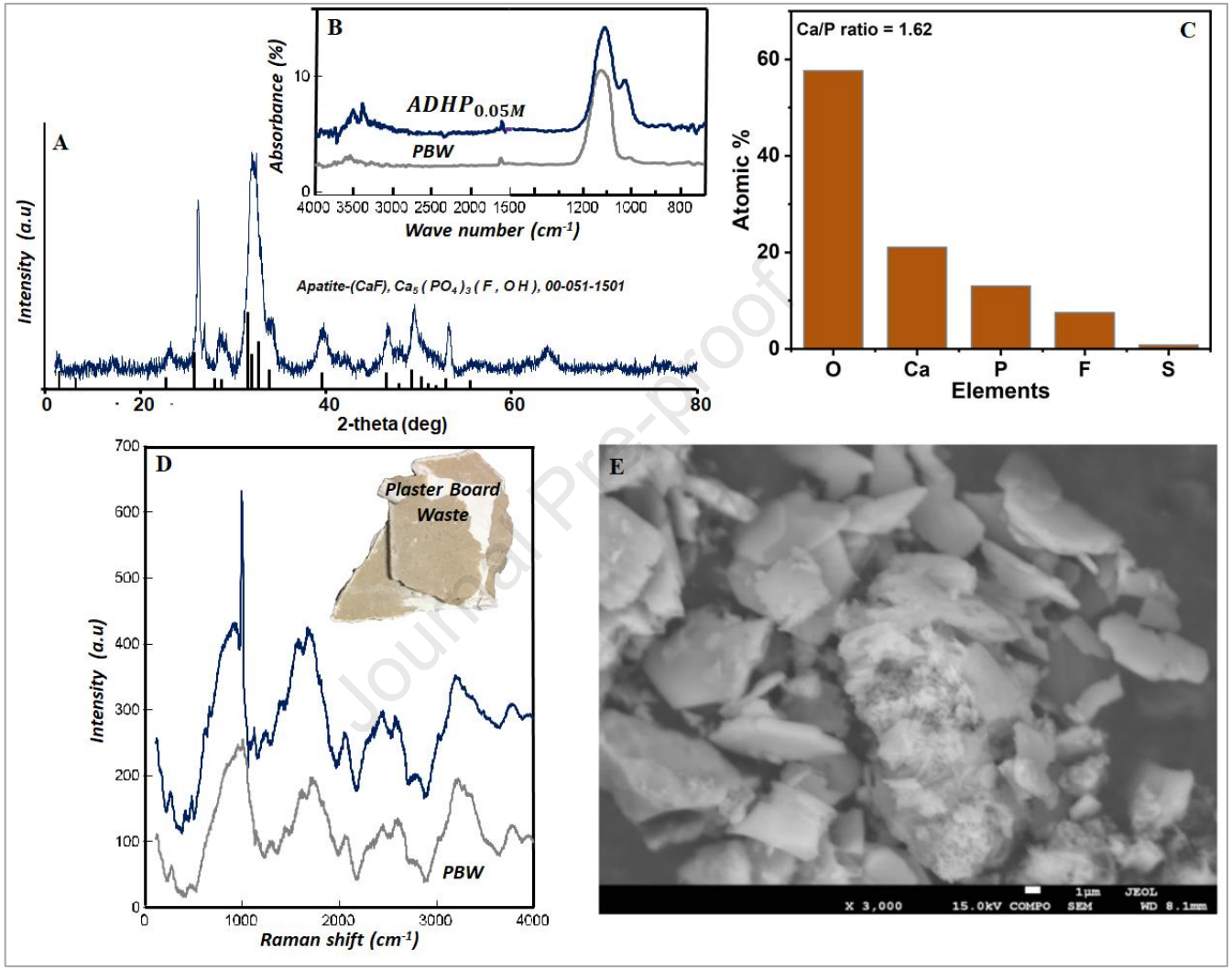

Fig. 5 Characterization results using XRD (A) FTIR (B) EDS (C) Raman (D) and SEM (E) for the synthesized fluorapatite from the treatment of recovered fluoride with PBW and DAHP

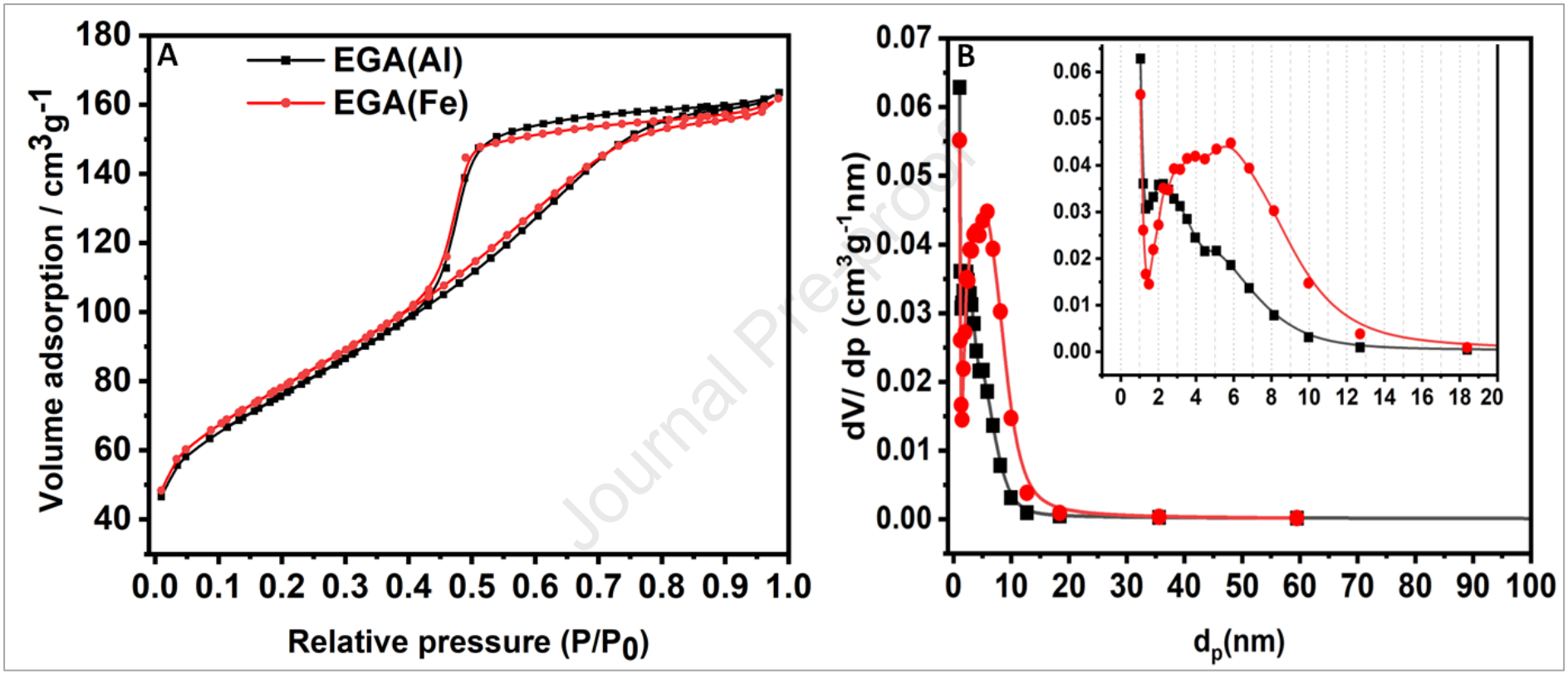

Fig. 6 N_2 adsorption−desorption isotherms (A) and pore size distribution of EGA adsorbents (B)

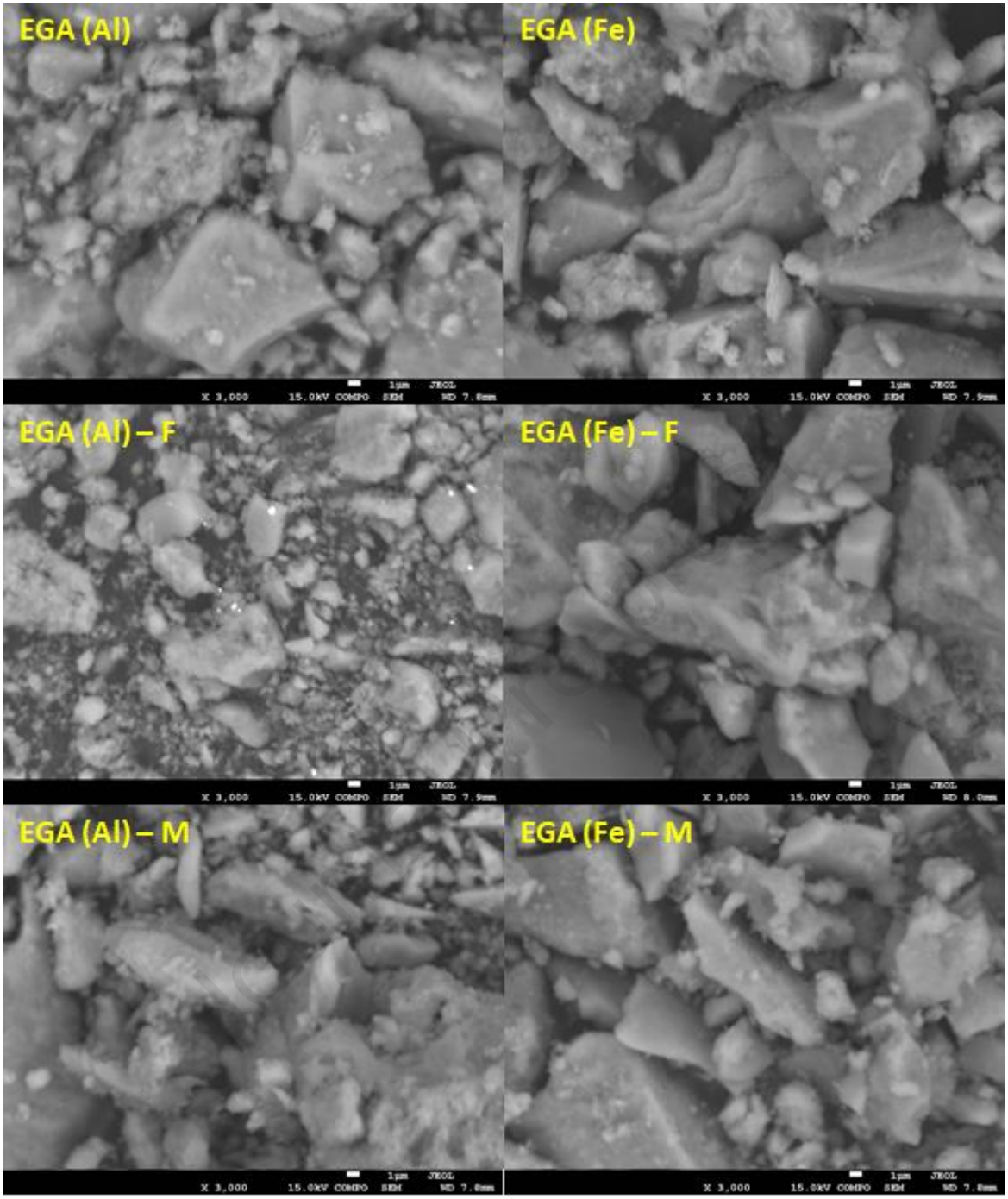

Fig. 7 Scanning electron micrographs of electro-generated alumina (EGAs)

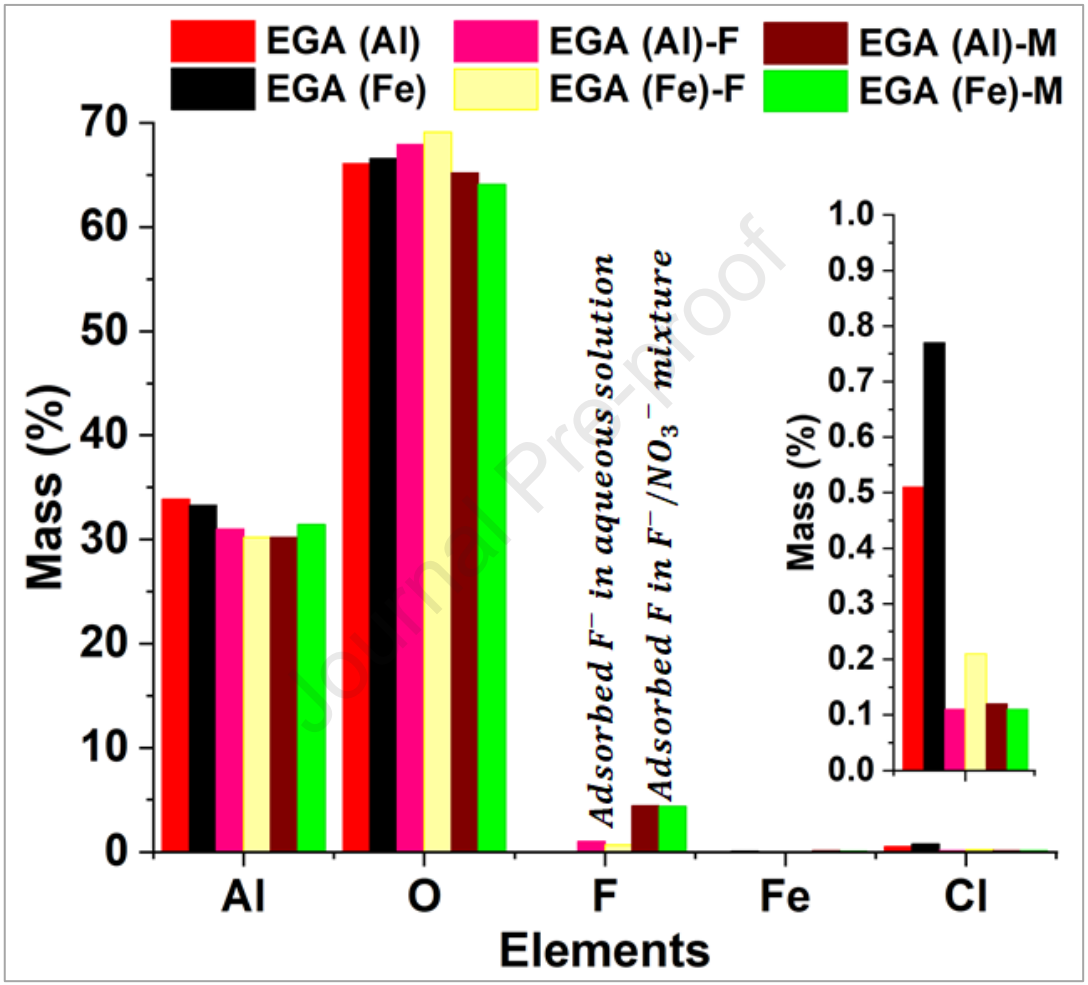

Fig. 8 Elemental dispersive spectroscopic analysis of EGAs

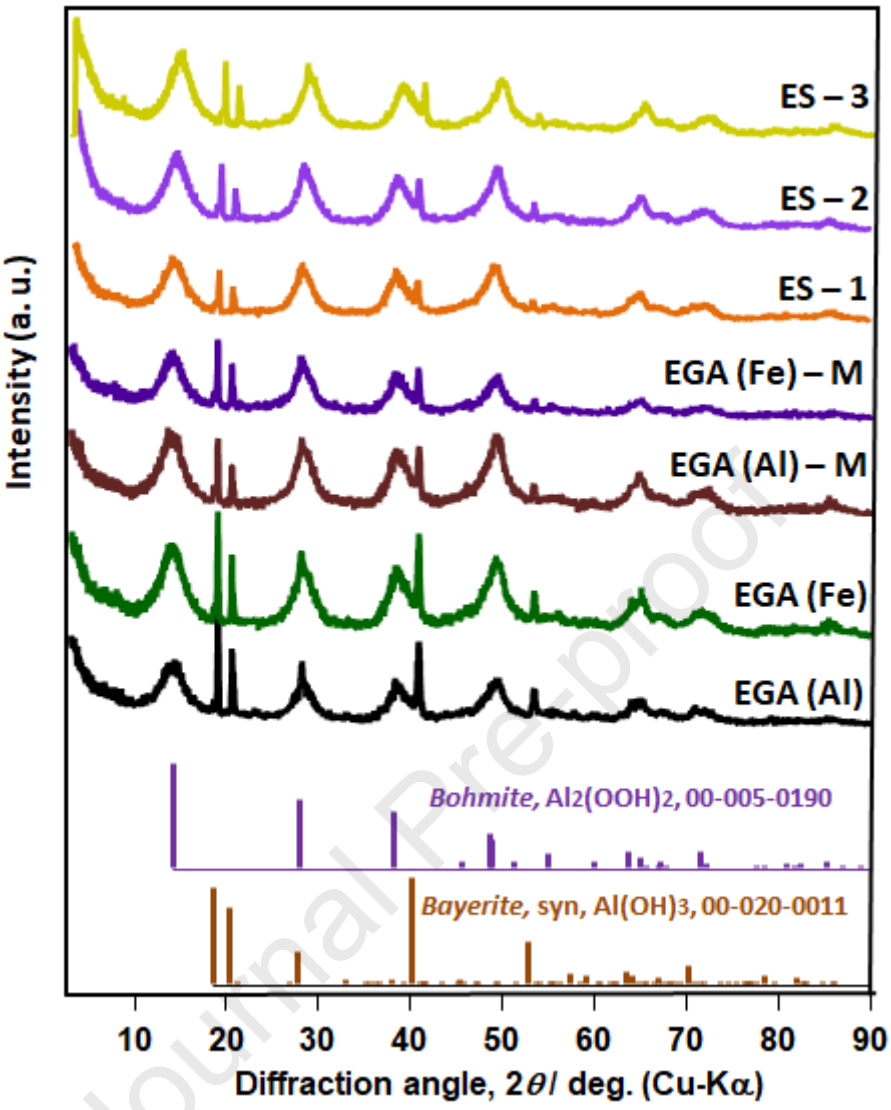

Fig. 9 X – ray diffraction patterns of EGAs

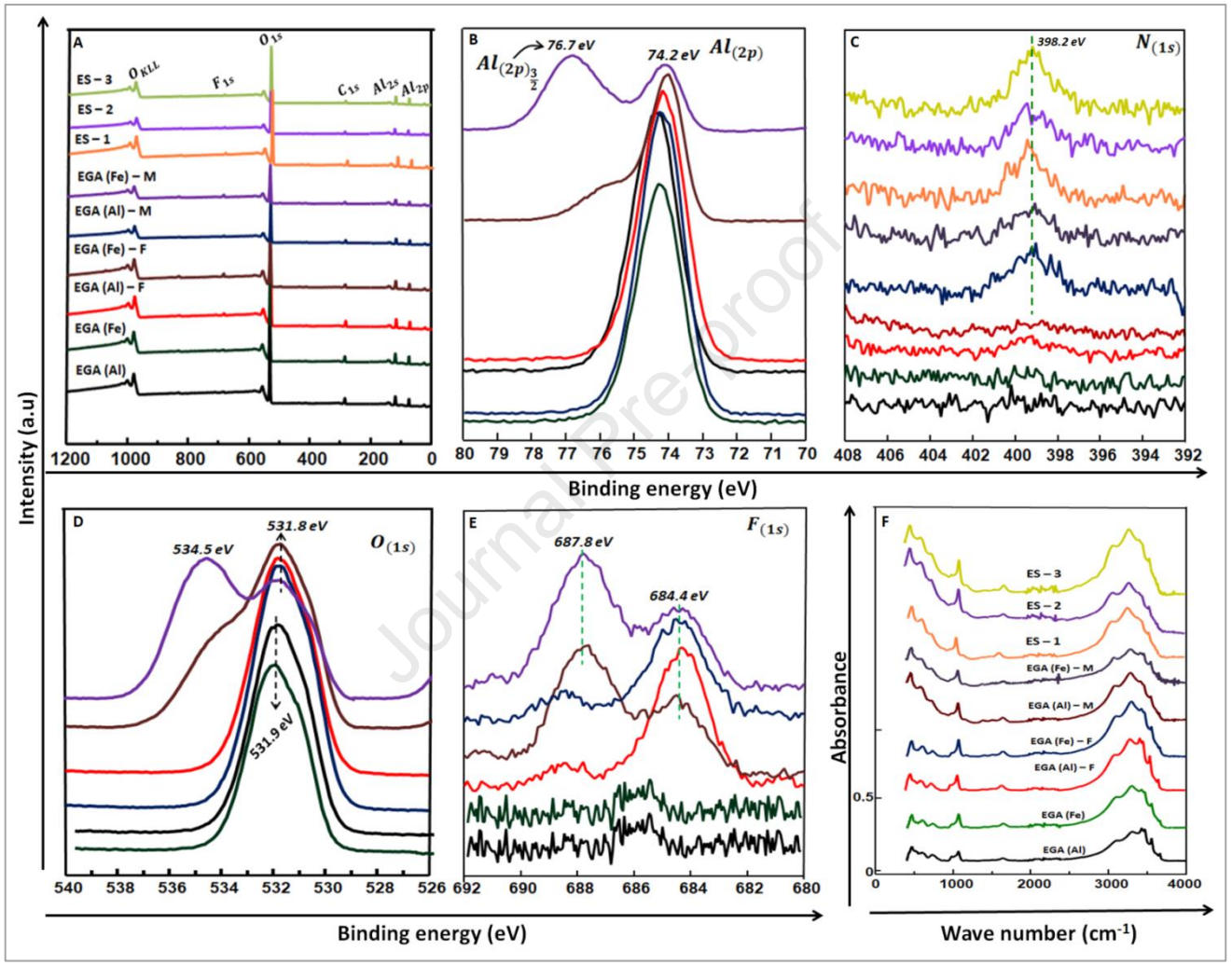

Fig. 10 X – ray photoelectron spectral (XPS) (A – E) and FTIR (F) patterns of EGAs

Research highlights

- Synthesized Electro-Generated Aluminas (EGAs) contain boehmite and bayerite phases
- The highest fluoride (99.50±0.04 %) and nitrate (83±1 %) removals were recorded
- The dominance of monolayer sorption of fluoride and nitrate ions was established
- XPS and TGA substantiated the substitution of hydroxyl by fluoride groups in boehmite
- The recovered fluoride was converted into fluorapatite

Declaration of interests

☒ The authors declare that they have no known competing financial interests or personal relationships that could have appeared to influence the work reported in this paper.

☐The authors declare the following financial interests/personal relationships which may be considered as potential competing interests:

T. Chaabane
V. Sivasankar